Self-tuning of neural circuits through short-term synaptic plasticity

David Sussillo[1] , Taro Toyoizumi[1] and Wolfgang Maass[2*†]
sussillo@neurotheory.columbia.edu, taro@neurotheory.columbia.edu,
maass@igi.tugraz.at

[1] Center for Theoretical Neuroscience in the Center for Neurobiology and Behavior,
Columbia University, New York, NY

[2] Institute for Theoretical Computer Science,
[*] http://www.igi.tugraz.at
Technische Universitaet Graz
A-8010 Graz, Austria

[†]Corresponding author

Abstract

Numerous experimental data show that cortical networks of neurons are not silent in the absence of external inputs, but rather maintain a low spontaneous firing activity. This aspect of cortical networks is likely to be important for their computational function, but is hard to reproduce in models of cortical circuits of neurons, since the low activity regime is inherently unstable. We show in this article through theoretical analysis and extensive computer simulations that short-term synaptic plasticity endows models of cortical circuits with a remarkable stability in the low-activity regime. This short-term plasticity works as a homeostatic mechanism that stabilizes the over all activity level in spite of drastic changes in external inputs and internal circuit properties, while preserving reliable transient responses to signals. The contribution of synaptic dynamics to this stability can be predicted on the basis of general principles from control theory.

Keywords

Dynamic synapses, self-tuning, network stability, control theory, cortical neural networks

Introduction

Cortical neurons fire not only in response to sensory inputs, but also spontaneously, as part of an ongoing network activity of the neocortex. According to (Steriade 2001), the rates of spontaneous firing recorded extracellularly from motor and association areas of awake monkeys and cats are typically in the range of 10 – 15 Hz. (Baddeley et al. 1997) found that cells in area IT (recorded extracellularly in awake macaque) fire at a rate of 14 (± 8.3) Hz during blank screen viewing. Intracellular recordings from regular spiking neurons (presumed to be pyramidal cells) in motor, association, primary somatosensory, and visual association areas of awake adult cats yielded a spontaneous firing rate of 9.4 (± 1.7) Hz (Steriade et al. 2001). The functional role of this spontaneous firing of neocortical neurons is unknown. It has been conjectured that persistent neuronal activity, which is "conspicuously absent in cerebellar and basal ganglia circuits", is an essential feature of the neocortex, which enables it "to incorporate the past into the system's present state" (Buzsaki 2006). It has also been conjectured to support "flexible cooperation among local and distant cell assembles", which is "believed to underlie the efficacy of cortical performance and is an essential ingredient for cognition" (Buzsaki 2006). On a more technical level, it has been pointed out that not only recurrent circuits of neurons in the neocortex, but dynamical systems in general support higher computational performance if they operate not in the ordered (or dissipative) regime, but closer to a critical state – which amounts to a substantial spontaneous firing activity in a neural circuit – so that also small external inputs can cause significant system responses ((Buzsaki 2006), (Legenstein and Maass 2007)).

Spontaneous brain activity is commonly assumed to be generated by a combination of intrinsic electrophysiological properties of single neurons and synaptic interactions in the network (see (Destexhe and Contreras 2006) for a recent review). But it had already been pointed out in (Abeles 1991) that "it seems to be very difficult to stabilize a network of inhibitory and excitatory neurons at very low levels of activity". We show in this article through theoretical analysis and extensive computer simulations that the short-term dynamics of synapses, more precisely the empirically found diversity of mixtures of paired-pulse-depression and paired-pulse-facilitation that depend on the type (excitatory or inhibitory) of pre- and postsynaptic neuron, endows networks of leaky integrate and fire (LIF) neuron models with either conductance based and current based synapses, with a remarkable stability of spontaneous network activity, even for rather low average firing rates – such as 10 Hz.

It is well-known that synapses in the neocortex do not respond to each spike in a train of spikes in the same way. Rather, the amplitude of the postsynaptic response (EPSP or EPSC) to a presynaptic spike depends on the history of presynaptic firing activity. If the response amplitude for the second spike in a pair of spikes is smaller than for the first one, one calls this effect paired-pulse depression. If the response amplitude for the second spike is larger, one calls this paired-pulse facilitation. But actually, most neocortical synapses exhibit a mixture of depression and facilitation, and the amplitude of the postsynaptic response depends in a complex manner on the temporal pattern of several preceding presynaptic spikes. This effect is commonly referred to as synaptic dynamics or short-term plasticity. In contrast to long-term synaptic plasticity this short-term plasticity does not usually depend on the pattern of postsynaptic firing, and its effect is not long lasting (more precisely: it only depends on the temporal pattern of presynaptic spikes during the last few seconds). We refer to (Abbott and Nelson 2003), (Thomson 2003), and (Abbott and Regehr 2004) for recent reviews of biological data and proposed functional roles of short-time synaptic plasticity. The dynamics of cortical synapses can be fitted quite well by the phenomenological model from (Markram et al. 1998), where the short-term dynamics of synapses is characterized by three parameters: U (which roughly models the release probability of a synaptic vesicle for the first spike in a train of spikes), D (time constant for recovery from depression), and F (time constant for recovery from facilitation). We call this set of parameters UDF herafter. An essentially equivalent model had been proposed in (Varela et al. 1997).

In contrast to the static synapse of an artificial neural network, a dynamic synapse does not just provide a fixed amplification of presynaptic activity, but rather implements a nonlinear filter that could potentially serve a number of different purposes, such as cortical gain control (Abbott et al. 1997), burst detection (Lisman 1997), or temporal integration of information (Maass et al. 2004), (Haeusler and Maass 2006). In (Tsodyks et al. 1998) it is was shown that depressing synapses can create in a mean field model for a population of excitatory neurons a stable fixed point for its activity, and that dynamic synapses can create a variety of rhythmic and irregular activity patterns if one adds a population of inhibitory neurons.

One intriguing aspect of biolocial data on synaptic dynamics is that this short term dynamics, more precisely: the parameters UDF, differ from synapse to synapse. More precisely, the UDF values form clusters within the 3-dimensional UDF parameter space, and the cluster to which the UDF-value of a particular synapse belongs depends on the type (excitatory or inhibitory) of its pre-synaptic neuron, and in some cases also on the type of the postsynaptic neuron (Thomson 1997), (Galarreta and Hestrin 1998), (Markram et al. 1998), (Gupta et al. 2000). It has been difficult to identify a possible functional role for the rules that assign a particular region in the 3-dimensional UDF parameter space to different types of synaptic connections. We show in this article that the assignment of different ranges of UDF values to different types of synapses makes it possible to implement a self-tuning principle for the firing rate of a cortical circuit. This self-tuning principle enables neural circuits to respond to external perturbations with a characteristic transient response in the firing rate of excitatory neurons, and then returns to its previous firing rate within a few 100 ms back into a given target range. The firing rate of inhibitory neurons is automatically adjusted by the synaptic dynamics so that it compensates the external perturbation. A similar self-tuning property can be demonstrated for changes within the circuit, such as those which are caused by long-term synaptic plasticity or changes in the concentration of neurotransmitters.

We show that this self-tuning principle in models of cortical networks of neuron is related to an abstract self-tuning principle that has recently been proposed for much simpler dynamical systmes in control theory (Moreau and Sontag 2003a), (Moreau and Sontag 2003b). Their abstract self-tuning principle enables some simple 2-dimensional dynamical system to return in a reliable manner to a particular operating regime (e.g. the vicinity of a bifurcation), in spite of external perturbations.). They considered the following dynamical system with external input $v(t)$ that has just two variables x (firing rate) and μ (synaptic strength):

$$\dot{x} = -\mu_0 x + \mu x + v(t) \tag{1}$$

$$\dot{\mu} = f(x) - g(\mu) . \tag{2}$$

The parameter μ_0 is here assumed to be unknown, and conditions[1] on the functions f and g are given under which the variable x moves (in the absence of external input) to a steady state x^* with $\dot{x} = 0$ (i.e., $\mu = \mu_0$) regardless of the value of this parameter μ_0. This system (1), (2) is obviously quite far away from models for recurrent neural networks consisting of excitatory and inhibitory neurons with nonnegative firing rates. However it is remarkable that its self-tuning property relies on the assumption that the strength μ of the positive feedback in (2) varies as a function of x, unlike the usual "static" synaptic weights in artificial neural networks. Furthermore the required assumptions on the functions f and g in (2) imply that μ decreases when x grows beyond its steady state value x^*. Hence the resulting dynamics of the "synaptic weight" μ has some properties in common with synapses between excitatory neurons in the cortex (which have been found to be usually depressing), although apparently no relation to synaptic dynamics had been intended (or even discussed) in (Moreau and Sontag 2003). We show in this article (see the end of Results, and the Supplementary Material) that this control principle can be generalized and adapted to more complex dynamical systems which consist of two interacting modules (e.g. a population of excitatory neurons and a population of inhibitory neurons) that have markedly different functional roles. It turns out, that an application of the control-principle to such a distributed system requires not only an activity-dependent modulation of "weights" $\mu(x)$, but *different* rules for the modulations $\mu_{mn}(x_n)$ of different weights, that depend on the type n of the source of the feedback $\mu_{mn}(x_n) \cdot x_n$ and the type m of the target of the synaptic connection (where m, n range over excitatory and inhibitory neurons). Hence in applications to models for cortical circuits, this principle requires differential synaptic dynamics for different types of synaptic connections.

More precisely, our theoretical analysis predicts that the UDF-parameters that characterize the dynamics of synapses belong to a specific region within the UDF-space (which we call the "N-volume") if a strengthening of this type of synaptic connection tends to increase the firing rate of excitatory neurons in the circuit, or into another region ("P-volume") if a strengthening of this type of synaptic connections tends to decrease the firing rate of excitatory neurons. A comparison of these predicted ranges of UDF values with empirically found UDF values gives a quite satisfactory (although not perfect) match. This is insofar remarkable, as many aspects that are relevant for the dynamics of cortical circuits of neurons (different input/output behaviours of excitatory and inhibitory neurons, further differentiation of neuronal dynamics according to subclasses of inhibitory (Gupta et al. 2000) and excitatory neurons, sub-networks formed by particular subtypes of neurons (Yoshimura et al. 2005) (Yoshimura and Callaway 2005), and modulation of neuronal dynamics through neuromodulators (Gulledge and Jaffe 1998; 2001)) are not reflected in the network models consisting of LIF neurons that we examine in this article.

Altogether this article provides a novel explanation for the functional role of short term synaptic dynamics, in particular also for the empirically found diversity of synaptic dynamics in dependence of the type of pre- and postsynaptic neurons. In addition it contributes new ideas and principles for the investigation of a research topic that is obviously of primary importance: the remarkable stability of cortical circuits of neurons against numerous perturbations and parameter drifts. This stability has so far neither been reproduced with artificial neural networks nor with biologically more realistic models for cortical circuits, hence an understanding of its prerequisites may provide important insight into design principles of cortical networks. The general program to investigate fundamental aspects of the design of neural circuits by focusing on their stability properties has already produced remarkable insight into another type of neural circuit: the pattern generating pyloric circuit in the crustacean stomatogastric ganglion, see (Marder and Goaillard 2006) for a recent review. It turns out that this circuit is endowed with intricate homeostatic

mechanisms that move a high-dimensional vector of internal parameters (conductances, etc.) to a different setting if one method for producing the desired firing pattern becomes unavailable, for example because of changes in the concentration of neuromodulators. Hence it is essential for the functioning of this pattern generating circuits that it can produce "multiple solutions to the production of similar behavior" (Marder and Goaillard 2006). We propose that analogous design principles are implemented in cortical circuits of neurons, which have to maintain a stable computational function in spite of drastic changes in the intensity of external inputs and in the concentrations of neuromodulators (that affect the excitability of neurons within the network (Gulledge and Jaffe 1998; 2001)). More specifically, we propose that the short-term dynamics of synapses is essentially involved in design principles that produce a stable function of cortical networks.

Materials and Methods

Neuron Models We used two leaky integrate and fire neuron models (LIF), one with current based synapses and the other with conductance based synapses. The current based LIF neuron is defined by

$$\tau_{mem} \frac{dV(t)}{dt} = -\left(V(t) - V_{rest}\right) + R_m \left(\sum_{j=1}^{K_E} j_{E,j}(t) + \sum_{j=1}^{K_I} j_{I,j}(t) + I^{ext}(t) \right), \tag{3}$$

where V is the membrane voltage, τ_{mem} is the membrane time constant, V_{rest} is the resting membrane voltage, R_m is the membrane resistance, $j_{E,j}(t)$ and $j_{I,j}(t)$ are the K_E and K_I synaptic currents from the excitatory and inhibitory synapses, respectively, and $I^{ext}(t)$ is an external input composed of mean input current, I^{inject}, and a white noise current $I^{noise}(t)$ with zero mean and standard deviation σ^{noise}. The LIF neuron with conductance based synapses is defined by

$$C_m \frac{dV(t)}{dt} = -g_{leak}\left(V(t) - V_{rest}\right) - \sum_{j=1}^{K_E} g_{E,j}(t)\left(V(t) - E_E\right) - \sum_{j=1}^{K_I} g_{I,j}(t)\left(V(t) - E_I\right) + I^{ext}(t), \tag{4}$$

where C_m is the membrane capacitance, g_{leak} is the leak conductance of the neuron, and $g_{E,j}(t)$ and $g_{I,j}(t)$ are the K_E and K_I synaptic conductances from the excitatory and inhibitory synapses, respectively. The constant E_E is the reversal potential for the excitatory synapses and the constant E_I is the reversal potential for the inhibitory synapses. The dynamics of each synapse over time are defined by

$$\frac{dj(t)}{dt} = -\frac{j(t)}{\tau_{syn}} + W\delta(t - t_{sp}), \tag{5}$$

where j is the instantaneous synaptic current or conductance, depending on the model, and W is the synaptic weight. The currents or conductances decrease exponentially with time constant τ_{syn} and increase instantaneously by adding W to the running value of $j(t)$ whenever a spike occurs in the pre-synaptic neuron at time t_{sp}. In this paper we compare the use of static synapses to dynamic synapses and so the synaptic weight W was constant in some simulations and in other simulations allowed to vary according to known biological rules of synaptic plasticity, i.e. $W(t)$. In the case of dynamic conductance based synapses we varied the maximal conductance and in the case of dynamic current based synapses we varied the maximal current. When static synapses were used (i.e. when W is constant) we use the notation J to denote the synaptic weight, and always state whether the simulation used conductance or current based synapses. When dynamic synapses were used (i.e. when $W(t)$ is implied) we use the notation μ to denote the synaptic weight.

We chose values for these LIF neurons that qualitatively reflect the high conductance, in-vivo UP state measured in in-vivo studies of cortical neurons (Destexhe et al. 2003). The membrane

resistance was $R_m = 10\text{M}\Omega$, the membrane time constant was $\tau_{mem} = 10\text{msec}$, in the case of neurons with conductance based synapses the capacitance was set $C_m = 10\text{msec}/10\text{M}\Omega = 1\text{nF}$. The neurons' resting potential was $V_{rest} = -60\text{mV}$ and the firing threshold $V_{thresh} = -50\text{mV}$. When the neuron spiked, the membrane voltage was reset to $V_{reset} = -60\text{mV}$, where it remained for a refractory period of $\tau_{refr} = 3\text{msec}$. The excitatory synaptic time constant τ_{syn} was $\tau_e = 4\text{msec}$, the inhibitory value was $\tau_i = 8\text{msec}$. In the case of neurons with conductance based synapses $g_{leak} = 1/R_m = 100\text{nS}$ and the reversal potentials for the excitatory and inhibitory neurons were $E_E = 0\text{mV}$ and $E_I = -80\text{mV}$. We modeled background synaptic inputs (from neurons outside of the simulated circuit) through $I^{ext} = I^{inject} + I^{noise}$ with a constant $I^{inject} = 2.455 \times 10^{-9}\text{Amp}$ and values of I^{noise} drawn from a 0-mean Gaussian with $\sigma^{noise} = 6 \times 10^{-9}\text{Amp}$ standard deviation. I^{ext} caused an average membrane potential of -55.4mV and standard deviation of 4.3mV in the absence of recurrent synaptic feedback (and when the threshold V_{thresh} was temporarily raised to 0mV in order to prevent spikes). This resulted in a firing rate around 20Hz for each neuron in the absence of recurrent synaptic input I^{rec} and was chosen as it is the median value of the firing rates of irregular and tonic discharges reported in in-vivo conditions in waking animals (Destexhe et al. 2003; Steriade et al. 2001) and is thus suitable for studying stability involving both up- and down-regulation of firing rates.
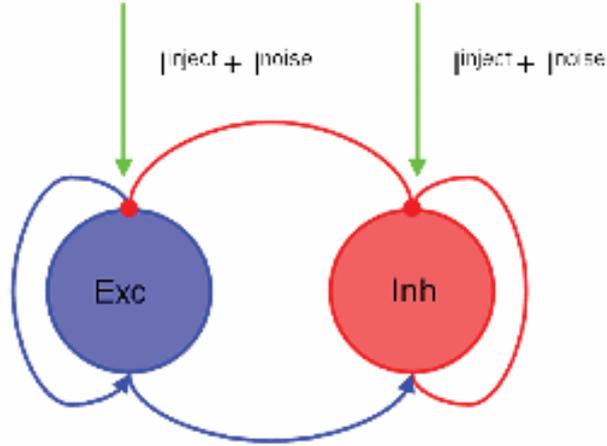

Figure 1 The basic network architecture used in mean-field simulations and spiking network simulations. Two populations of neurons connect to each other, one excitatory Exc with firing rate x_e and one inhibitory Inh with firing rate x_i. The color blue denotes excitatory populations or recurrent excitatory connections and the color red denotes inhibitory populations or inhibitory recurrent connections. If the synaptic connections have a static synaptic weight they are denoted J_{mn} from pre-synaptic pool n to post-synaptic pool m, if the synaptic connections have dynamic synaptic weights then they are denoted as μ_{mn}. External excitatory input is labeled $I^{inject} + I^{noise}$ and is denoted by the color green. The external input in this paper is a constant noisy current with a stationary mean.

Spiking Network Model In our simulations we created sparse, random spiking networks of 5000 neurons with 4000 excitatory neurons and 1000 inhibitory neurons. Neurons were either excitatory or inhibitory. The network models contained either purely LIF neurons with conductance based synapses or purely LIF neurons with current based synapses, we refer to the former as "conductance based networks" and the latter as "current based networks". We use the term sparse to denote that the number of excitatory connections K_e and inhibitory connections K_i to a given

neuron are much less than both the total number of excitatory neurons N_e or inhibitory neurons N_i in the network. We use the term random to denote that the connections between neurons are chosen randomly and follow no other design principle. Following (Vogels and Abbott 2005) the neurons were connected randomly to each other with a 2% connection probability. The network connectivity between neuron types is shown in figure 1.

Dynamic Synapse Model We used two equivalent forms of dynamic synapse models for networks with spiking and non-spiking neurons. The first set of equations (6) is taken from (Markram et al. 1998)[2] and describes for the case of spiking neurons the magnitude of the synaptic weight μ_k (a current or conductance, depending on the network model) for the kth spike in a spike train with inter-spike intervals $\Delta_1, \Delta_2, ..., \Delta_{k-1}$:

$$
\begin{aligned}
\mu_k &= AR_k u_k \\
u_k &= U + u_{k-1}(1-U)\exp(-\Delta_{k-1}/F) \\
R_k &= 1 + (R_{k-1} - u_{k-1}R_{k-1} - 1)\exp(-\Delta_{k-1}/D) \\
u_1 &= U \\
R_1 &= 1,
\end{aligned}
\tag{6}
$$

where u is the running variable for synaptic utilization and R is the running variable for synaptic availability, with u, $R \in [0,1]$. The constants U, D and F (for curtness further denoted as UDF, or $AUDF$ when the strength scaling factor A is included) represent the release probability for the first spike, the depression time constant and facilitation time constant, respectively. The synaptic weight for the kth spike is then defined by μ_k (i.e. $W := \mu_k$ in equation (5)) and has an arbitrary strength scale set by A.

An equivalent, continuous mean-field model for dynamic synapses was developed in (Tsodyks et al. 1998), which can be used in non-spiking mean field models with continuous time. The mean-field equations for dynamic synapses are given by

$$
\begin{aligned}
\mu &= ARU^1 \\
\dot{u} &= -\frac{u}{F} + U(1-u)x(t) \\
\dot{R} &= \frac{1-R}{D} - U^1 R\, x(t) \\
U^1 &= u(1-U) + U
\end{aligned}
\tag{7}
$$

where $x(t)$ represents the instantaneous firing rate of the pre-synaptic neuron, U^1 is simply an algebraic term introduced for clarity, and μ, u, R, U, D and F have the same meaning as in equations (6). Note the magnitude $\mu(t)$ of the synaptic weight at time t depends not only on the current pre-synaptic firing rate $x(t)$, but through the auxiliary variables u and R also on the history of this pre-synaptic firing rate.

The steady-state equations for this continuous dynamic synapse model yield in the case of a constant pre-synaptic firing rate $x(t) = x^*$

$$
\begin{aligned}
\mu^* &= AR^* U^{1*} \\
u^* &= \frac{FUx^*}{1 + FUx^*} \\
R^* &= \frac{1}{1 + DU^1 x^*} \\
U^{1*} &= u^*(1-U) + U,
\end{aligned}
\tag{8}
$$

where the * notation denotes steady-state values of u, U^1, R and μ. In particular for $m,n \in \{e,i\}$ $\mu_{mn}^*(x_n)$ defined according to (8) denotes the *steady-state synaptic weight* from any neuron in population n to any neuron in population m as a function of the pre-synaptic firing rate $x^* = x_n$.

Table 1

		U	D (sec)	F (sec)
R1	EE	0.5939	0.5333	0.1828
	EI	0.4028	0.0016	0.0848
	IE	0.0007	0.1153	0.1795
	II	0.5089	0.1744	0.4973
R2	EE	0.6319	0.9468	0.9949
	EI	0.1517	0.0063	0.2701
	IE	0.0746	0.0001	0.9043
	II	0.3029	0.4429	0.9963
R3	EE	0.5762	0.6187	0.7989
	EI	0.1010	0.0105	0.1003
	IE	0.0865	0.0004	0.5779
	II	0.5521	0.6139	0.4220
Experimental	EE	0.59	0.813	0.001
	EI	0.049	0.399	1.79
	IE	0.16	0.045	0.376
	II	0.25	0.706	0.021

Table1 R1, R2 and R3 - UDF parameters were chosen randomly based on theoretical criteria (see Methods). The UDF parameters for synapse types $E \rightarrow I$ and $I \rightarrow E$ were randomly chosen from the P-volume (figure 4), and the UDF parameters for synapses $E \rightarrow E$ and $I \rightarrow I$ were chosen randomly from the N-volume.
Dynamic synapse parameters from experimental literature -U, D and F values . The $E \rightarrow E$ and $E \rightarrow I$ synapse types had UDF values taken from the means given in (Markram et al. 1998). The $I \rightarrow E$ and $I \rightarrow I$ had UDF values taken from the means given in (Gupta et al. 2000). The F1 (facilitating) parameters were used for $I \rightarrow E$ synapses and the F2 (depressing) parameters were used for $I \rightarrow I$ synapses.

Linking UDF Parameters to Network Stability We show that the fundamental property of dynamic synapses for creating a network with a stable firing rate is the relationship between the slopes of the steady-state synaptic weight curves $\mu_{mn}^*(x_n)$ for different synapse types. We searched for UDF parameters that generate a negative derivative for the connections $E \rightarrow E$ and $I \rightarrow I$ because for our parameters an increase in the strength of either leads to a higher firing rate x_e of the excitatory neurons, and a positive derivative for the steady-state curves for the connections $E \rightarrow I$ and $I \rightarrow E$ because an increase in their strengths leads to a lower firing rate x_e (see Supplemental Materials for further explanation). More specifically, we searched for UDF settings that generated either a strictly positive or strictly negative derivative between the frequencies 10Hz and 100Hz of the pre-synaptic firing rate and that additionally were in a physiological range (see table 1). We uniformly sampled the UDF space in the range $U \in (0,1]$, $D \in (0,1]$ sec and $F \in (0,1]$ sec (at increments of 0.014 in each dimension), and found two topologically simple volumes of parameter space which satisfied these requirements. These were named "P-volume" for the positive derivative

and the "N-volume" for the negative derivative. We randomly chose three assignments R1, R2, R3 to the UDF values of the four synapse types to create three separate dynamic synapse UDF parameters sets. Thus each parameter set $R_i (i=1,2,3)$ consisted of two points from the N-volume, which were randomly assigned as mean for the UDF-parameters of the synaptic connections $E \rightarrow E$ and $I \rightarrow I$, and two points from the P-volume, which were also randomly assigned as mean to the synaptic connections $E \rightarrow I$ and $I \rightarrow E$. Each individual R_i parameter set was used separately from the others in the network simulations. Additionally, we used experimental data on UDF parameters from (Gupta et al. 2000; Markram et al. 1998) for all four synapse types, see table 1. All self-tuning simulations were carried out for these parameters based on experimental data, as well as all three parameter assignments R1, R2, R3 based on a theoretical analysis of desirable network performance. Performance differences between the R1-R3 parameter settings were small, and we averaged the responses across the parameters sets. These UDF-parameters were fixed for all self-tuning experiments, and only the scaling factors A_{mn} of the dynamic synapses were modified on a per-simulation or per-network basis.

Altogether synaptic parameters were chosen as follows. All synapses were given a uniform delay of 0.1msec. The means of the scaling factor parameters (the A s in equations (6) and (7)), mean UDF parameters, and mean values for the initial conditions for dynamic synapses $u0$ and $R0$ were set as described above. After selection of a mean value, each actual value was drawn for each synapse in the network from a Gaussian distribution with a standard deviation of 10% of the mean value (e.g. all UDF parameters for every synapse were chosen from a Gaussian distribution with a standard deviation equal to 10% of the mean UDF parameters, which depended on the synapse type). If the actual value would have been set below zero, then the value was redrawn from a uniform distribution between zero and two times the mean.

Self-tuning Simulation Setup The self-tuning simulations we performed involved measuring and comparing the equilibrated (steady-state) average firing rates of excitatory neurons with static synapses and then with dynamic synapses for three network models: conductance based networks, current based networks and a rate-based mean-field network (see below for the definition). There were three types of perturbation simulations run, with two parameters perturbed in each case:
- mean input current strength and standard deviation of current injection
- excitatory synaptic strength and inhibitory synaptic strength
- percentage excitatory neuron inactivation (a temporary cessation of function potentially caused by a variety of circumstances such as neuromodulators) and percentage inhibitory neuron inactivation.

This resulted in 841 networks for the input perturbation experiments, and 900 networks for the synaptic weight perturbation and neuronal inactivation experiments. Each network was generated with random connections and first run in the control case with static synapses. The network was then regenerated with the exact same parameters, but a different random number seed, and run with dynamic synapses. In order to test the robustness of the ideas presented, each network was tested with four different dynamical synapse parameters sets, three based on theoretical considerations called R1, R2 and R3 and the parameters based on experimental data, thus requiring $841 + 841 \text{ x } 4 \text{ x } 3 = 10,933$ separate network simulations for the input perturbation experiments and $900 + 900 \text{x} 4 \text{ x } 3 = 11,700$ separate network simulations for experiments with synapse strength and neuronal inactivation perturbations. To measure the firing rates we let the control networks with static synapses run for 1500msec and the average firing rates of excitatory and inhibitory neurons were measured for the last 1000msec. The networks with dynamic synapses ran for 2000msecs, and the steady-state firing rates were measured for the last 1000msecs, which allowed extra time for the dynamic synapses to equilibrate. The measured firing rates for the theoretically derived UDF-values were then averaged across all three dynamic synapse parameters sets R1, R2 and R3. Network simulations were performed using the CSIM neural simulator (Natschläger et al. 2003)

and MatLab (The MathWorks Natick, MA). The simulation time step was 0.1 milliseconds. The mean-field simulations were also performed using MatLab.

Correlation Function Network synchrony plays a large role in the behavior of networks of sparsely connected, spiking neurons (Brunel 2000). We were interested in separating asynchronous irregular activity from other types of network activity. We used the voltage traces of randomly sampled neurons to analyze the network correlation and then applied the standard cross covariance function. The covariance coefficient for the sequences y and z, with means $\bar{y}$ and $\bar{z}$, defined at the zeroth lag, is given by

$$C_{yz}(0) = \frac{\sum_{n=0}^{N-1}(y_n - \bar{y})(z_n - \bar{z})}{\sqrt{\sum_{n=0}^{N-1}|y_n - \bar{y}|^2 \sum_{n=0}^{N-1}|z_n - \bar{z}|^2}}.$$

To measure the network correlation, we created two random groups of neurons from the excitatory neuron population (excepting differences in firing rate, the inhibitory neurons behave in same manner as the excitatory neurons). The two groups each had $5\% = 250$ neurons in them. The cross covariance coefficient was computed for every pair of neurons, one from each group, (excluding identical neurons which occurred by chance) and the average cross covariance coefficient was taken as a measure of the network correlation.

Mean-field Models for Sparsely Connected Neural Circuits We have developed for our analysis of network stability neuronal population models (i.e., mean-field firing rate models) for sparse, random networks (van Vreeswijk and Sompolinsky 1996), (van Vreeswijk and Sompolinsky 1998). They model populations of current based neurons with static and dynamic synapses, and are based on a balance of excitation and inhibition that creates temporally irregular spiking. We assume that there are N_e excitatory neurons and N_i inhibitory neurons. K_{mn} is the number of synaptic connections from neurons in pool n to neurons in pool m (we assume that $K_{mn} << N_e, N_i$). We are interested in networks with randomly chosen sparse synaptic connections because they provide reasonable first approximation models for cortical circuits.

As the firing rate of a neuron is dependent on both the mean input current and the variance of the input current, we refer to its input-output function as the FMS (Firing rate, Mean input, Standard deviation) surface, which we denote by F. A sparse, random network has a parameter range that allows for asynchronous irregular activity (Brunel 2000), or see (Vogels et al. 2005) for a review, and the synaptic currents to a given cell are uncorrelated in time for this regime, aside from a potentially fluctuating population firing rate. In the steady-state condition, that is when all the dynamics of the system have been allowed to equilibrate, this allows one to use the time average of the synaptic input for estimating the synaptic input at each point in time. Thus in the asynchronous condition, and assuming Poisson spiking statistics, one can write down the average recurrent synaptic current I^{rec} and recurrent synaptic input variance σ^{rec2} for each neuron in their respective

$$I_m^{rec} = \sum_n K_{mn}\tau_n x_n J_{mn}$$

pools m (Shriki et al. 2003) as   (9)

$$\sigma_m^{rec2} = \frac{1}{2}\sum_n K_{mn}\tau_n x_n J_{mn}^2,$$

where $m, n \in \{e, i\}$ represent indices into the post- and pre-synaptic pools, respectively. So the total average current and total input current variance into a neuron in a pool m is

$$I_m^{tot} = I_m^{rec} + I^{inject} + I^{noise}$$

$$\sigma_m^{tot2} = \sigma_m^{rec2} + \sigma^{inject2} + \sigma^{noise2},$$ (10)

where I^{inject} and σ^{noise2} represent the mean and variance of external input to the neuron, and I_m^{tot} and σ_m^{tot2} are the mean and variance of the total current injection to each cell (see Methods).

In order to use these formulas to create a working neuron model one can easily sample the FMS surface of a single current-based neuron by injecting current with an arbitrary mean and Gaussian noise component, and then use the equations (9) to translate the parameters $(J_{ee}, J_{ei}, x_e, J_{ei}, J_{ii}, x_i)$ into (I^{tot}, σ^{tot}). Using this technique we sampled the FMS surface F of a current-based LIF neuron with the same neuronal parameters as the neurons used in our current-based spiking networks. Using the samples generated from this neuron we used smoothing splines to create a nonparametric approximation $\overline{F}$ to F that could be evaluated at any given point to yield a good approximation of the post-synaptic firing rate (figure 2).
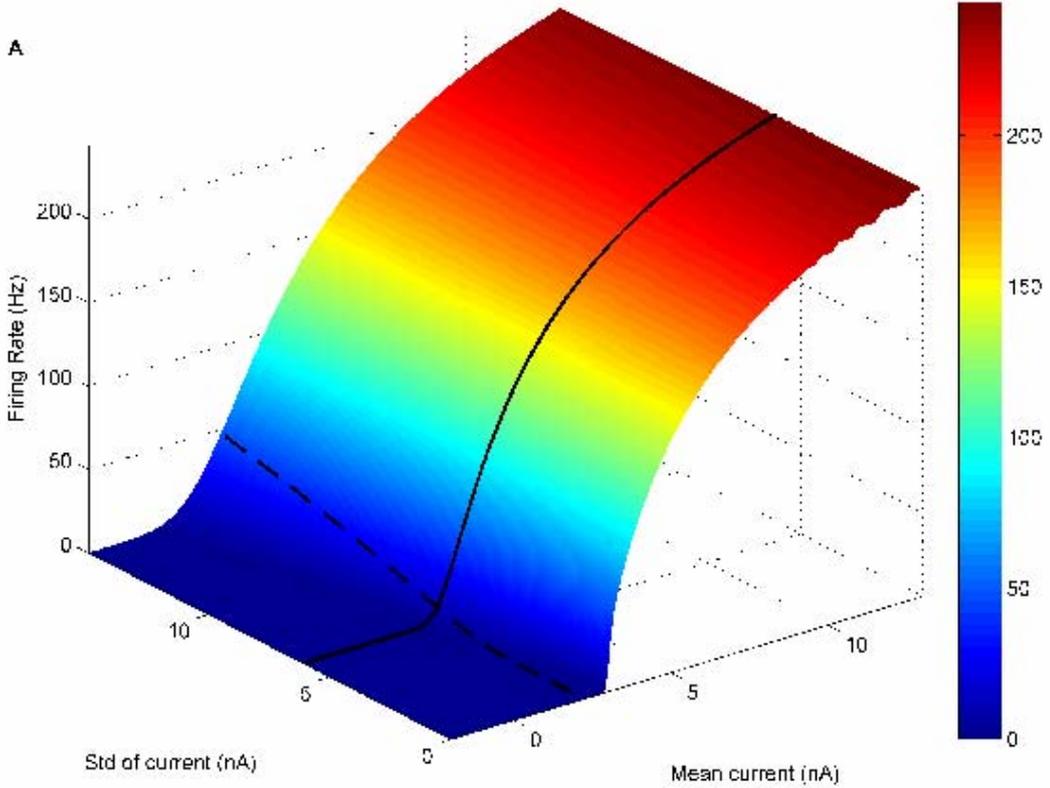

Figure 2 FMS Surface for LIF neuron. **A** The approximated FMS (Firing rate, Mean current injection, Standard deviation of current noise injection) surface $\overline{F}$ of LIF neuron with $\tau_m = 10\text{msec}$, $\tau_{rp} = 3\text{msec}$, $V_{rest} = -80\text{mV}$, and $V_{reset} = -60\text{mV}$. The approximated $\overline{F}$ gives a very good fit, mean absolute error 0.2Hz. The dashed black line shows the firing rate as a function of the external current noise level assuming a constant current injection of $2.455 \times 10^{-9}\text{Amp}$. The solid black line shows the firing rate as a function of mean input, with injected noise value of $6 \times 10^{-9}\text{Amp}$. The intersection of these two lines denotes the external input (mean current and noise level) that every neuron in all simulations of spiking neurons received, and resulted in a steady-state firing rate of 20Hz in the absence of synaptic feedback.

As the excitatory and inhibitory neurons in our current based networks have the same neuronal parameters, we used the same neuron model for both types. Finally, the mean-field model for a network of excitatory and inhibitory neurons in an asynchronous network, which also represents a sparse, random network under the same assumptions, is defined by

$$\tau_{mem} \frac{dx_e}{dt} = -x_e + \overline{F}(I_e^{tot}, \sigma_e^{tot})$$

$$\tau_{mem} \frac{dx_i}{dt} = -x_i + \overline{F}(I_i^{tot}, \sigma_i^{tot}),$$

(11)

where x_e is the average firing rate of the excitatory neurons and x_i is the average firing rate of the inhibitory neurons. For a current-based LIF network with $\tau_e, \tau_i < \tau_{mem}$, the correct time constant of the model is the neuronal membrane time constant τ_{mem}.

This model can also be used to analyze system dynamics, even though the equations in (11) were developed from an analysis of the steady-state, since the neuronal dynamics of a current-based neuron acts merely as a low pass filter. A major assumption of this approach is that all combinations of $(J_{ee}, J_{ie}, x_e, J_{ei}, J_{ii}, x_i)$ lead to asynchronous, irregular network firing, which is not always the case for sparse, random spiking networks. Thus, in order for the mean-field model to correctly predict the behavior of the spiking network, the range of parameters must be limited to assure this assumption, and consequently the network correlation and coefficient of variation (CV) of inter-spike intervals were measured.

Finally, we introduce dynamic synapses (equations (7)) into the sparse, random mean field model of equations (11). The model is defined by equations (11) with slightly different definitions for I_m^{rec} and σ_m^{rec2}

$$I_m^{rec} = \sum_n K_{mn} \tau_n x_n \mu_{mn}(x_n, t)$$

$$\sigma_m^{rec2} = \frac{1}{2} \sum_n K_{mn} \tau_n x_n \mu_{mn}(x_n, t)^2,$$

(12)

where have replaced the static synaptic weight value J_{mn} with the dynamic synaptic weight value $\mu_{mn}(x_n, t)$.

Results

Conditions on Dynamic Synapses to Create Network Stability The goal of introducing dynamic synapses into the sparse, random model is to set up a stable fixed point at a desired target network firing rate $x_e = x_i = x^*$, so that x_e is robust to various types of perturbations, i.e. the circuit is self-tuning. We view self-tuning as the ability of a system to ultimately return a system value to given range, despite a perturbation in system parameters or input. We define the output of the network to be the average excitatory firing rate, x_e, which is the firing rate that is actively controlled, perhaps by increasing or decreasing x_i. While sparse, random networks also have steady-state firing rates as a function of static synaptic weight values J_{mn}, we will show that introducing dynamic synapses with relatively general constraints endows the network with much greater robustness under a variety of perturbations. This improved robustness is achieved if the UDF parameters (the parameters of the dynamic synapse model, see Methods) of the dynamic synapses are chosen to satisfy the following three conditions[3]:

- maintain the synaptic weight values if the pre-synaptic firing rate is equal to the desired firing rate,
- increase the strength of the $E \rightarrow E$ and $I \rightarrow I$ synapses and decrease the strength of the $E \rightarrow I$ and $I \rightarrow E$ synapses if the pre-synaptic firing rate is below the target firing rate,
- decrease the strength of the $E \rightarrow E$ and $I \rightarrow I$ synapses and increase the strength of the $E \rightarrow I$ and $I \rightarrow E$ synapses if the pre-synaptic firing rate is above the target firing rate.

The first constraint involves creating the fixed point at a target firing rate by setting the scaling factor A of the dynamic synapse model according to the formula

$$A_{mn} = \frac{J_{mn}}{R^*_{mn}(x^*)U^{1*}_{mn}(x^*)},$$ (13)

where J_{mn} are specific synaptic weight values of a corresponding network with static synapses, and $R^*_{mn}(x^*)$ and $U^{1*}_{mn}(x^*)$ are the steady-state values for the internal dynamic synapse variables as a function of pre-synaptic firing rate, here set to the desired steady-state firing rate. (see equations (6) (7) in Methods). Equation (6) and (11) ensure that the steady-state dynamic synapse weight is equal to the static synaptic weight ($\mu^*_{mn}(x^*) = J_{mn}$) for a pre-synaptic firing rate x^*. We refer to $\mu^*_{mn}(x^*)$ as the steady-state value for μ_{mn} (see the Methods, equation (8)), and call it the resulting function of x^* the *steady-state synaptic weight curve* (see figure 3).
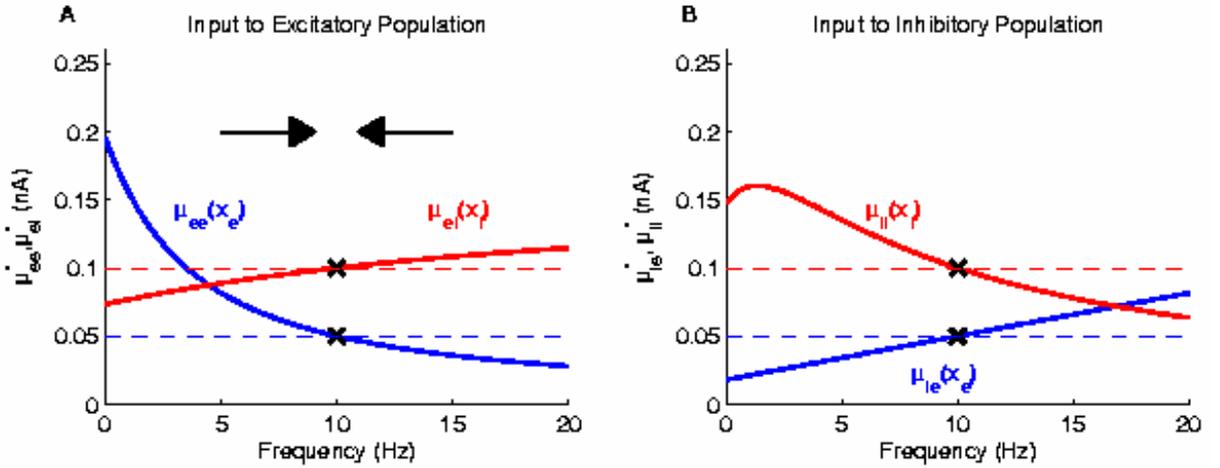

Figure 3 The steady-state synaptic strengths μ^*_{mn} are used to control the excitatory firing rate in a network with dynamic synapses. **A** The synaptic strengths to the excitatory population as a function of pre-synaptic firing rate. The dashed, straight lines show static synapse values such that $x_e = x_i = 10\text{Hz}$ (blue – J_{ee}, red – J_{ei}). The thicker, curved lines show the dynamical synapse steady-state strengths tuned such that exactly at 10Hz (black 'X'), the static and dynamic synapse values match up (blue – $\mu_{ee}(x_e)$, red – $\mu_{ei}(x_i)$) and therefore a network with dynamic synapses also supports the 10Hz excitatory and inhibitory firing rate of the network with static synapses. **B** Same as A but for the inhibitory population. Note the inversion of the slopes of the steady-state synaptic strengths. Dashed, straight lines - (blue – J_{ie}, red – J_{ii}). Thicker, curved lines - (blue – $\mu_{ie}(x_e)$, red – $\mu_{ii}(x_i)$). The arrows in panel A show how the dynamic synapses will push the excitatory firing rate towards 10Hz in the event of a system perturbation. If a perturbation causes x_e to increase, then $\mu_{ee}(x_e)$ decreases (panel A) and $\mu_{ie}(x_e)$ increases (panel B), thereby causing a decrease in x_e and an increase in x_i. The latter induces an increase in $\mu_{ei}(x_i)$, causing an additional decrease in x_e via x_i. If a perturbation causes x_e to decrease then the same curves explain an increase in x_e.

In the asynchronous range, when static synaptic weight values $(J_{ee}, J_{ei}, J_{ie}, J_{ii})$ are set for a sparse, random network, the network has a specific steady-state firing rate associated with those synaptic strengths, x^* (van Vreeswijk and Sompolinsky 1996; 1998). Since the network already has a fixed point with firing rate x^* for these static weights, we simply scale the dynamic synapses to take these static weights at x^*. We do this by setting the value of A_{mn} according to equation (13), which gives $\mu^*_{mn}(x^*) = A_{mn}R^*_{mn}(x^*)U^{1*}(x^*) = J_{mn}\left(R^*_{mn}(x^*)U^{1*}(x^*)/R^*_{mn}(x^*)U^{1*}(x^*)\right) = J_{mn}$, thus returning the firing rate x^*.
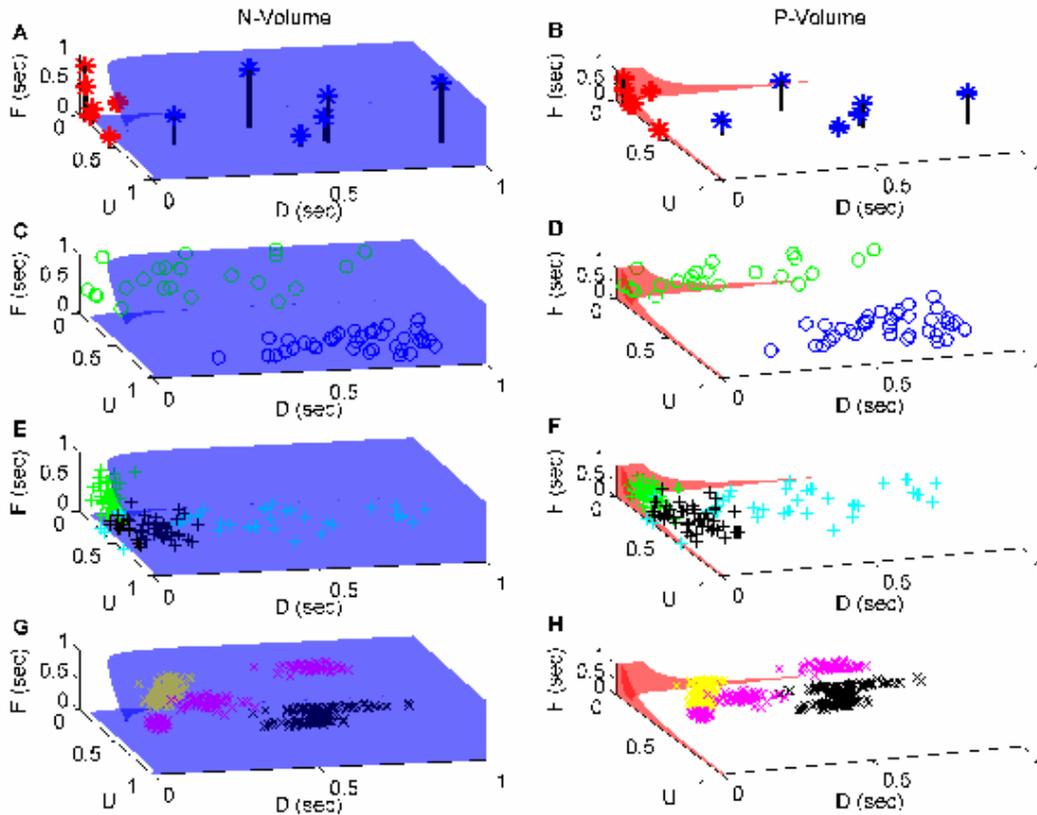
Figure 4 Two volumes in the UDF parameter space where the steady-state synaptic weights $\mu_{mn}^{*}(x_{mn})$ have either positive or negative derivatives with respect to pre-synaptic firing rate, which are essential for the theoretical prediction of resulting self-tuning properties of the resulting network. **A-B** Randomly generated UDF parameters ($E \to E$ and $I \to I$ denoted by blue '*' and $I \to E$ and $E \to I$ denoted by red '*') which are used to test the theoretically predicted stability properties of UDF values from these two volumes. A - The "N-Volume" of UDF space (blue) denotes that parameter range in which $\mu^{*}(x_{pre})$ has a negative derivative between the firing rates of $10\mathrm{Hz}$ and $100\mathrm{Hz}$ (also in C, E, G). **B** The "P-Volume" of UDF space (red) denotes that parameter ranges in which $\mu^{*}(x_{pre})$ has a positive derivative between the firing rates of $10\mathrm{Hz}$ and $100\mathrm{Hz}$ (also in D, F, H). **C-D** Sampled UDF values for pyramid to pyramid (blue circles) and pyramid to interneuron (green circles) connections based on means and standard deviations from (Markram et al. 1998). **E-F** Sampled UDF values for F1 facilitating synapses (green '+'), F2 depressing synapses (cyan '+') and F3 recovering synapses (black '+') based on means and standard deviations from (Gupta et al. 2000). These are all UDF values of GABAergic synapses whose targets are either excitatory or inhibitory neurons. Hence no clear prediction for the ranges of their values can be made through the proposed theoretical analysis. The UDF values of F1 and F2 synapses to lie close to the border region between the P- and N-volume. **G-H** Sampled UDF values for medial prefrontal cortex excitatory to excitatory synapses (PFCe1, PFCe1a, PFCe1b samples as yellow 'x', PFCe2, PFCe2a, PFCe2b samples as black 'x' and PFCe3, PFCe3a, PFCe3b samples as magenta 'x') based on means and standard deviations from (Wang et al. 2006). All these UDF values lie in the N-volume, as predicted by the theoretical analysis.

Satisfying the second and third constraints involve setting the UDF parameters of the dynamic synapses such that if there is a perturbation in the network that affects the steady-state firing rate then the dynamic synapses attempt to compensate and bring x_e back to x^{*}. The UDF parameters are responsible for the shape of the steady-state synaptic weight curve. Hence, in order to create an attractor at x^{*}, which produces firing rate stability, we choose UDF parameters such that the synapse types $E \to E$ and $I \to I$ have negative derivatives in their steady-state synaptic weight curves and the synapse types $E \to I$ and $I \to E$ have positive derivatives in their steady-state synaptic weight curves (see figure 3.) In order to test the validity of this analysis, we ran a

parameter search over the range of physiological UDF values to determine whether there were simple volumes of UDF space that fulfill these two requirements through the range of firing rates $10 - 100\,\text{Hz}$. (See the Methods for a description of how and why these values were chosen). Based on these theoretical considerations we chose 3 sets of UDF parameters (R1, R2 and R3) for each of the 4 synapse types randomly from the appropriate sub-volume of UDF space: For synaptic connections $E \rightarrow E$ and $I \rightarrow I$ six points were chosen from the blue N-volume, for $E \rightarrow I$ and $I \rightarrow E$ six points were chosen from the red P-volume, see figure 4 panels A and B. All resulting UDF parameters are listed in table 1. The three conditions explained above create a stable fixed point for the firing rates of the resulting dynamical system (see figure 3). At the target firing rate $x_e = x_i = x^*$, the dynamic synapses equilibrate to $\left(J_{ee}, J_{ei}, J_{ie}, J_{ii}\right)$, which maintains the firing rate. At a firing rate less than x^* the synapses $E \rightarrow E$ and $I \rightarrow I$ increase their synaptic weight values to values greater than J_{ee} and J_{ii} and the synapses $E \rightarrow I$ and $I \rightarrow E$ decrease their strength to less than J_{ei} and J_{ie}, leading to an increased excitatory firing rate. At a firing rate greater than x^* the synapses $E \rightarrow E$ and $I \rightarrow I$ decrease their synaptic weight values to less than J_{ee} and J_{ii} and the synapses $E \rightarrow I$ and $I \rightarrow E$ increase their synaptic weight values to greater than J_{ei} and J_{ie}, leading to a decreased excitatory firing rate.

In addition, we took experimentally found UDF values reported in (Markram et al. 1998) and (Gupta et al. 2000), and compared their contribution to network stability with that of the theoretically deduced parameters that were selected as previously described. We sampled random points from Gaussian distributions with means and standard deviations as reported in these articles, and plotted the resulting UDF values in figure 4, panels C-F. The UDF values for $E \rightarrow E$ synapses from (Markram et al. 1998) (blue circles in figure 4 panels C and D) lie clearly in the N-volume. The UDF values for $E \rightarrow I$ synapses from that study lie much closer to the P-volume, but are not contained in it. The UDF values of GABAergic synapses of type F1 (facilitating), F2 (depressing), and F3 (recovering) reported in (Gupta et al. 2000) are contained in the N-volume (see green, cyan, and black crosses in figure 4 panels E and F), but those for type F1 and F3 are close to the P-volume. This ambiguous position of UDF-parameters for GABAergic synapses could be related to the fact, that from a theoretical perspective for improved homeostatic plasticity the $I \rightarrow I$ and $I \rightarrow E$ connections may have either positive or negative derivatives depending on other network parameters (see Supplemental Materials) In (Wang et al. 2006) several additional clusters of UDF values for $E \rightarrow E$ synapses in prefrontal cortex are reported. These values (plotted in figure 4 panels G and H) all fall clearly into the N-volume (into which they should fall according to the proposed theoretical analysis).

Network Parameter Ranges In order to find ranges of synapse strengths for static synapses that were compatible with low firing rates and low network correlation in current based or conductance based networks, we varied the excitatory and inhibitory synaptic weights of conductance based and current based networks (see Methods and figure 5).

Specifically, we varied two synaptic weight values, one excitatory synaptic weight J_e and one inhibitory synaptic weight J_i, and set the all synaptic weight values such that $J_{ee} = J_{ie} = J_e$ and $J_{ei} = J_{ii} = J_i$. So that results between conductance and current based networks could be compared we scaled the conductance based synapses so that the conductance and current based synapses had equal strength when the conductance based synapses were multiplied by their respective driving forces at the neurons' resting potential. We found a broad parameter range of synaptic weights which could potentially support dynamic synapses as a network feedback mechanism in the asynchronous, irregular regime. However, since we measured the firing rate, network correlation, and coefficient of variation of the interspike interval (ISI CV) for only a two dimensional manifold of the four dimensional space of synaptic weights $\left(J_{ee}, J_{ei}, J_{ie}, J_{ii}\right)$, these parameter maps serve only as a guide with which to start our simulations, since the parameter space becomes four

dimensional when the dynamic synapses are allowed to vary the synaptic strengths according to individual dynamic synapse formulas with different AUDF parameters. We always started our networks with synaptic weight initial conditions from these two dimensional maps, so that the networks started in a setting where the network behavior is asynchronous irregular and the feedback current magnitudes are on par with or smaller with the level of the background current injection. Based on these maps, we used the synaptic weight parameter range shown in figure 5 (panels A, D and G) as the starting point for the rest of our conductance and current based spiking network simulations, as well as our sparse, random mean-field simulations of equations (11), all of which used dynamic synapses. Specifically. $J_{ee}, J_{ie} \in [0, 0.1] \times 10^{-9} \, \text{Amp}$, and $J_{ei}, J_{ii} \in [-0.2, 0] \times 10^{-9} \, \text{Amp}$ for current based spiking networks and the current based mean field model and $J_{ee}, J_{ie} \in [0, 1.67] \times 10^{-9} \, \text{S}$, and $J_{ei}, J_{ii} \in [0, 10] \times 10^{-9} \, \text{S}$ for the conductance based spiking networks and the dynamic synapses were set to these values using equation (13).
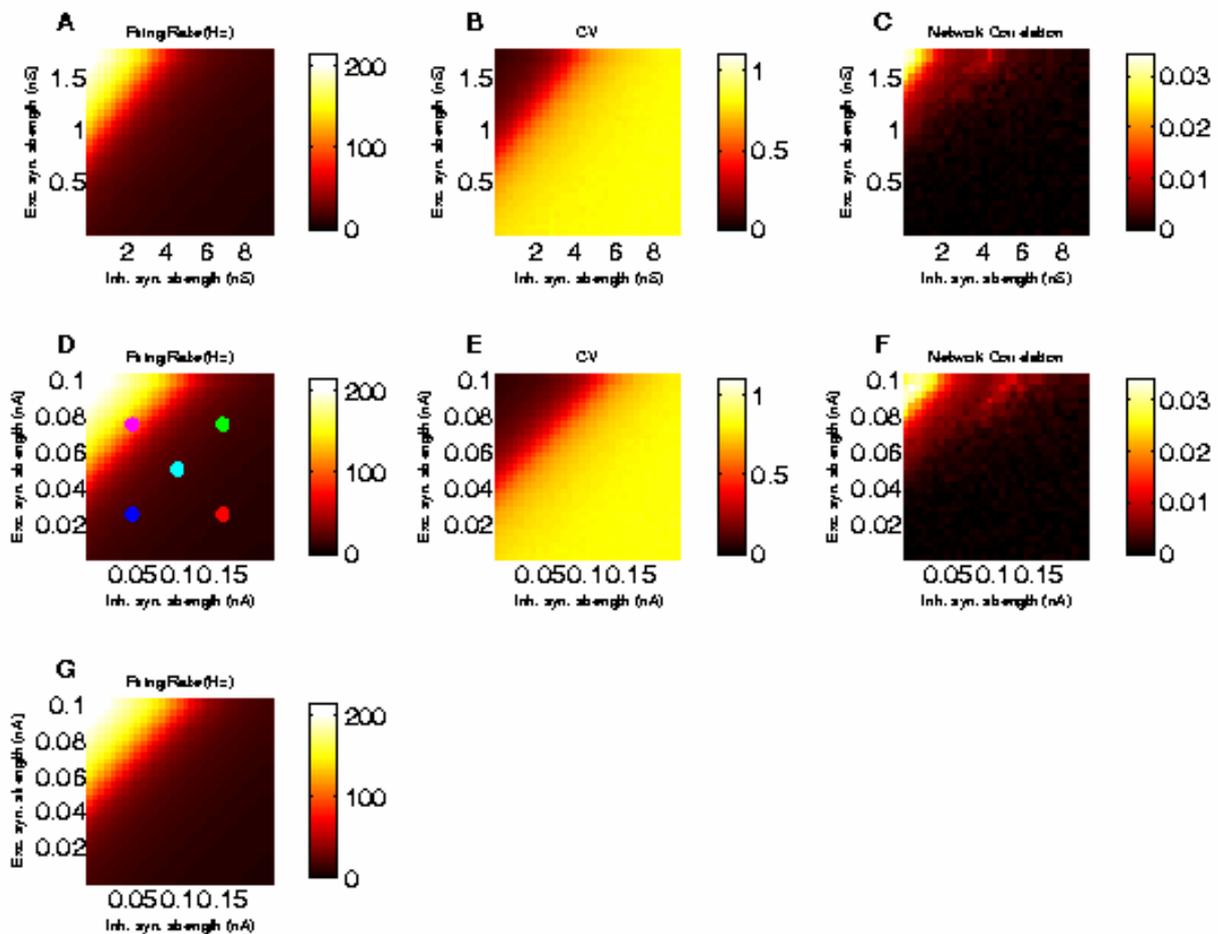

Figure 5 Parameter search over synaptic weights for conductance based spiking networks, current based spiking networks and mean-field firing rate networks with static synapses. The Y axis is $J_e = J_{ee} = J_{ie}$ and the X axis is $J_i = J_{ei} = J_{ii}$. **A-C** Network statistics for conductance based spiking networks with static synapses. A - Network steady-state firing rate. B – Coefficient of variation (CV) for conductance based spiking networks over the range of synaptic weights. C Network correlation of excitatory population as measured as described in the Methods section. There was no significant network correlation. **D-F** Network statistics for current based spiking networks with static synapses. D – Network steady-state firing rate. The 5 colored circles represent the current based spiking network settings used in the target firing rate simulation. E – CV for current based spiking networks over the range of synaptic weights. F – Network correlation of excitatory population. There was no significant correlation over the range of synaptic weights tested. **G** – Network steady-state firing rate for mean-field firing rate model.

As a verification of our current based mean-field model (9) – (11) without dynamic synapses, we used the same settings as in the networks of current based spiking neurons (see figure 5, panel G) for the mean-field model and compared the average firing rate. The mean-field model was in excellent agreement with the current based spiking network simulations across the very wide parameter range sampled, with a mean absolute error (MAE) of 0.8Hz and a maximum error of 3.8Hz over the parameter range.
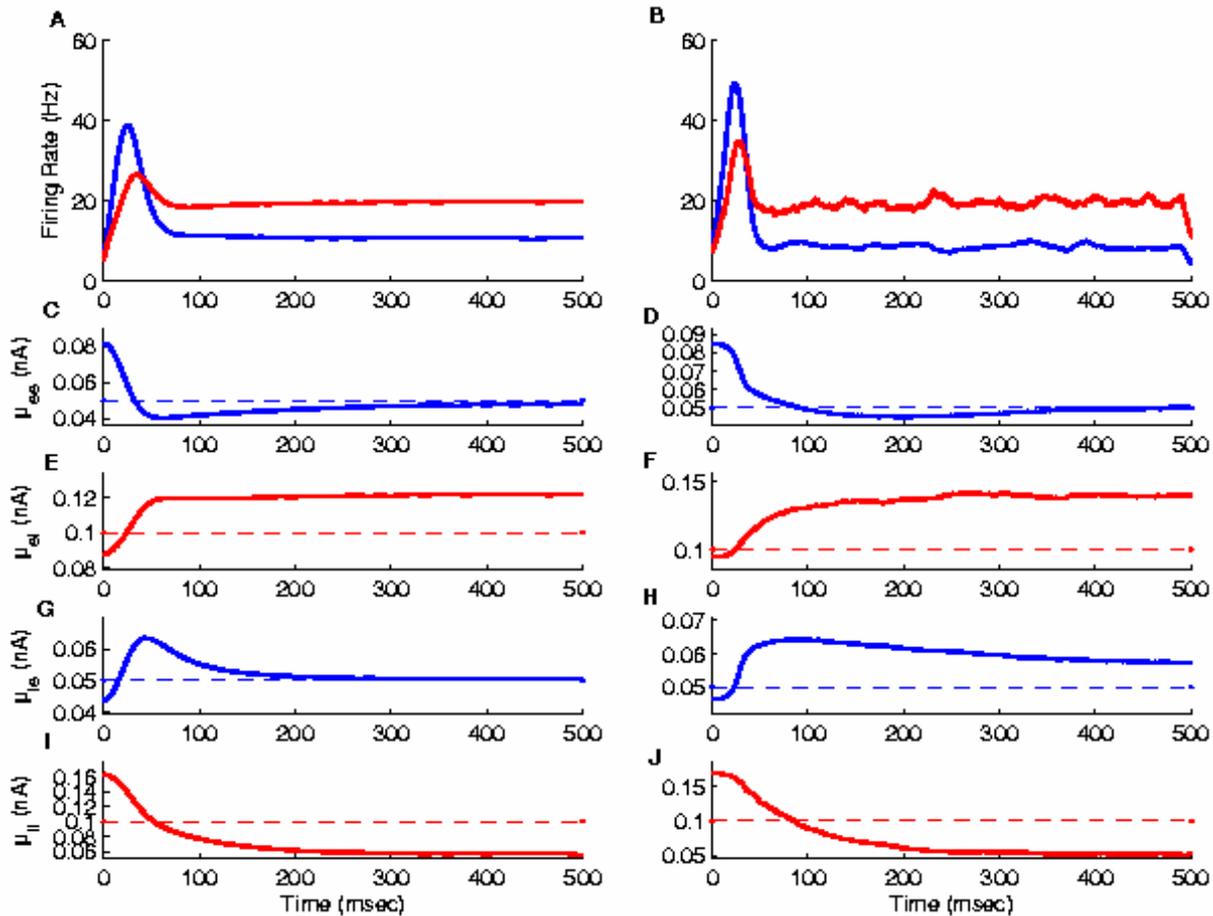

Figure 6 Example showing the firing rates and synaptic weights over time to demonstrate the effect of dynamic synapses on the network firing rate. The scaling factors A_{mn} were set such that the desired steady-state firing rate is 10Hz, even though the synaptic weight values $[J_e, J_i] = [0.5, -1] \times 10^{-10} \text{Amp}$ gave a steady-state firing rate of 20Hz without dynamic synapses. Initial conditions of the dynamic synapses were set to values corresponding to 5Hz steady-state firing rate. **A** Firing rate curve of mean-field model, x_e in blue, x_i in red. **B** Firing rate curve of network simulation, the firing rate is smoothed with a low pass filter (box car filter with length equivalent to 20msec). The two firing rate curves are in good qualitative agreement (the drop in firing rates at 500msec is only a filtering artifact). **C-J** Synaptic weights through time as set by the dynamic synapse equations. C, D μ_{ee}. E, F μ_{ei}. G, H μ_{ie}. I, J μ_{ii}. C, E, G, I Mean-field model. D, F, H, J Spiking network model. The dashed lines represent the values J_{ee}, J_{ei}, J_{ie}, and J_{ii}. A comparison of the panels on the left and right hand side shows a good agreement between the mean-field model and the spiking network.

Interaction of Synaptic Dynamics with Network Activity In order to give an idea of how dynamic synapses interact with the network, we discuss an example in detail. The example, see figures 6 and 7, shows a burst in a network of current based spiking neurons followed by a convergence to a steady-state firing rate (a conductance based example would work nearly identically, except that the effect on the synaptic conductances would be harder to visually interpret due to the effect of the driving force on each synapse). We also show a sparse, random mean-field

simulation using the same parameters. A network was chosen that normally fires at 20Hz in the absence of dynamic synapses, $J_{ee} = J_{ie} = 0.05 \times 10^{-9} \text{Amp}$ and $J_{ei} = J_{ii} = -0.1 \times 10^{-9} \text{Amp}$. The network was initialized with the dynamic synapse parameter initial conditions set to a 5Hz steady-state firing rate and the desired firing rate for the network was set to 10Hz, by adjusting the scaling factors A_{mn} in equation (8). The firing rate initial conditions for the network were also set to 5Hz, as best as possible. Since a firing rate of 5Hz gives an overall positive network gain when the target firing rate is set to 10Hz, the firing rate shot up at the beginning of the simulation (figure 6 panels A, B) . The dynamic synapses adapted to this new firing rate and brought it back down, ultimately reaching nearly the steady-state of 10Hz for the excitatory population, while the inhibitory population firing rate remained near 20Hz. Thus we see that an excitatory firing rate very near the target firing rate x_e^* was reached from quite different initial conditions, and then maintained. During the simulation, the average dynamic synapse weights were modified and caused the changes shown in the firing network firing rates (figures 6 panels C-J) . We can assert that the dynamic synapses caused the change in network firing rate (and not the other way around) because the time constants of the dynamic synapses are much longer than any neuronal time constants. Again there is excellent agreement between the current-based mean field model and the current based spiking network simulation.
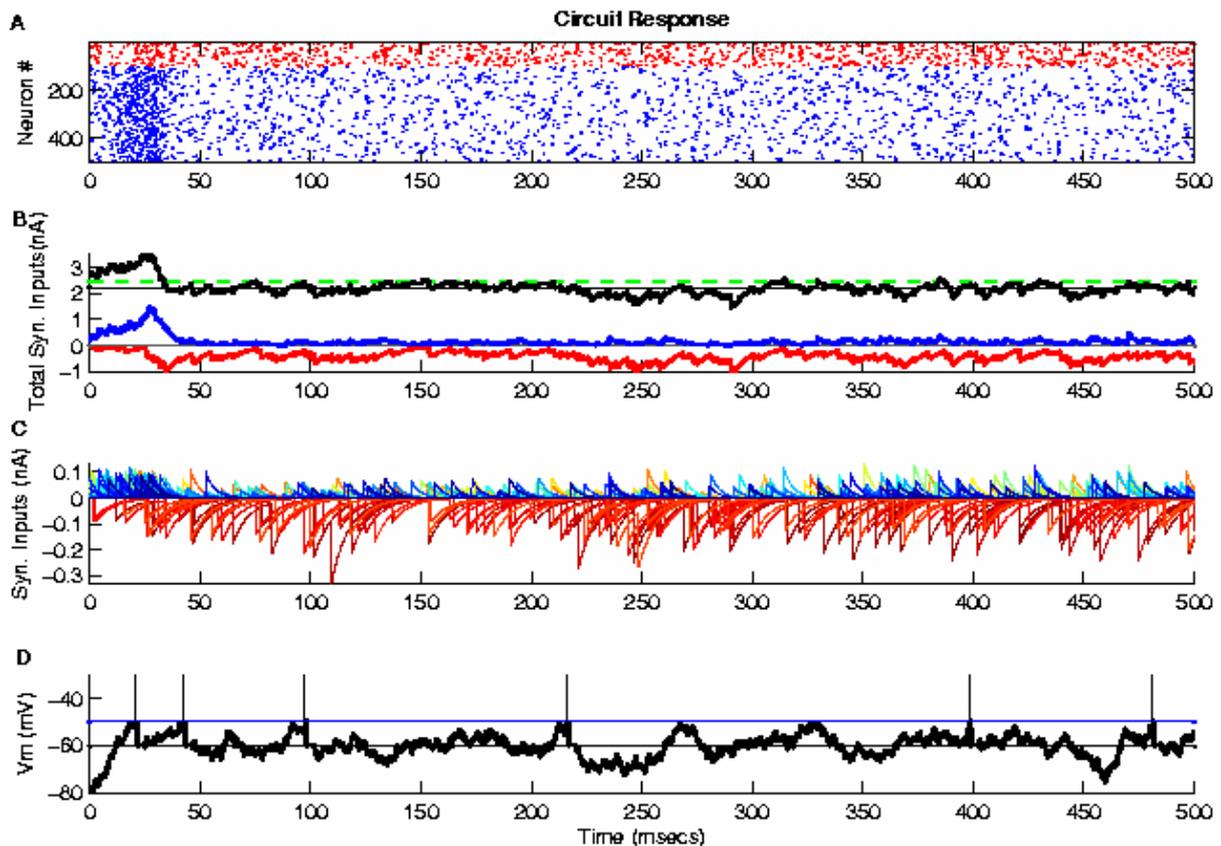

Figure 7 Detailed analysis of network activity in the network example from figure 6. **A** Spike raster showing the spiking activity of 500 neurons (out of 5000), 400 excitatory and 100 inhibitory. Panels B, C, D show data from a single excitatory neuron. **B** Total synaptic excitatory and inhibitory currents. The blue line shows the total excitatory input over time, the red line shows the total inhibitory input over time. The black line shows the total amount of current into the neuron excluding the noise injection. The green dashed line shows the mean current injection into the neuron, which corresponds to a 20Hz firing rate in the absence of synaptic feedback. **C** Individual synaptic currents (each color represents a separate synapse to the neuron). The individual synaptic currents are plotted to give an idea of changes in synaptic weight values. Upward exponential curves represent excitatory currents and downward, inhibitory currents. The peak values of these currents are set by the dynamic synapses and vary roughly over two times the magnitude of the average current. **D** Membrane potential of the selected neuron, with action potentials. The thick black line represents the membrane potential of the cell, the thin black line represents the average. The blue line shows the neuron's firing threshold.

A spike raster of a random subset of neurons in the current based spiking network example are shown in figure 7, panel A. It shows that the network functioned in the asynchronous range, aside from correlation induced by a common network firing rate. Panels B-D show data from a single example neuron in the simulation. The total synaptic current hovered around the background current and the recurrent synapses subtly influenced this current. When the network achieved the steady-state firing rate, the total current was slightly below the normal background current (panel B), thus creating a average firing rate of 10Hz as opposed to the 20Hz without dynamic synapses. The individual synaptic currents are shown in panel C, which show differences in magnitude of 3-4 times as a result of the short-term plasticity.
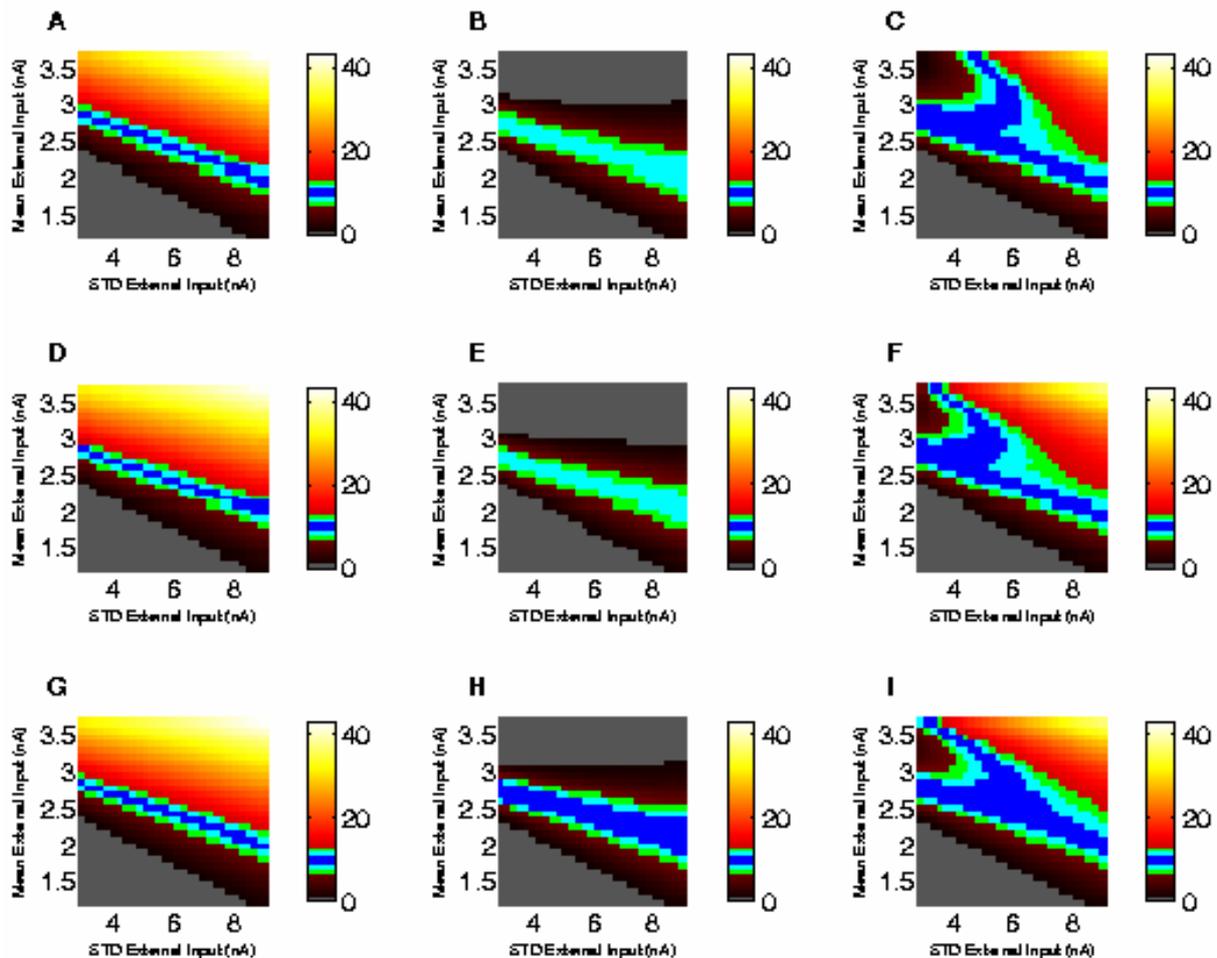

Figure 8 Self-tuning with respect to perturbations of the level and variance of external input currents. All networks tested were set to a default steady-state firing rate of 10Hz. The scaling factors A_{mn} were set only once, thus each set of simulations (a single panel) where dynamic synapses were used, had identical synapse parameters. The color blue denotes the optimal firing rate of 10Hz (between 9Hz and 11Hz), cyan between $8-9\text{Hz}$ and $11-12\text{Hz}$, green between $7-8\text{Hz}$ and $12-13\text{Hz}$ and gray denotes networks between $0-1\text{Hz}$. **A-C** Networks with conductance based synapses. A – The response (average excitatory firing rate) of conductance based networks with static synapses to perturbations of external current mean and noise. B – The averaged response of conductance based networks over dynamic synapse parameters R1-R3. C – The response of conductance based networks with the dynamic synapse parameters based on experimental data. **D-F** Networks with current based synapses. D - The response of current based networks with static synapses to perturbations of external current mean and noise strength. E – The averaged response of current based networks over dynamic synapse parameters R1-R3. F – The response of current based networks with the dynamic synapse parameters based on experimental data. **G-I** The response of a current based mean-field networks. G – The response of current based mean-field model with static synapses to perturbations of external current mean and noise strength. H – The averaged response of mean-field networks over dynamic synapse parameters R1-R3. I – The response of the mean-field networks with the parameters based on experimental data.

Self-tuning in Networks of Spiking Neurons To investigate the self-tuning properties of dynamic synapses on spiking networks we asked whether dynamic synapses could help tune a spiking neural network to a steady-state target firing rate even if the external input was perturbed, as it occurs for example in primary sensory areas of the cortex in response to sensory stimuli. In order to test this, we used a conductance based spiking network ($J_{ee} = J_{ie} = 0.4 \times 10^{-9} \text{S}$ and $J_{ei} = J_{ii} = 8.48 \times 10^{-9} \text{S}$), a current based spiking network ($J_{ee} = J_{ie} = 0.013 \times 10^{-9} \text{Amp}$ and $J_{ei} = J_{ii} = -0.18 \times 10^{-9} \text{Amp}$) and a current based mean-field models ($J_{ee} = J_{ie} = 0.013 \times 10^{-9} \text{Amp}$ and $J_{ei} = J_{ii} = -0.18 \times 10^{-9} \text{Amp}$), all with a steady-state firing rate of 10Hz. We additionally performed all of our self-tuning tests with the current based mean-field model because it aids us in understanding the self-tuning properties of networks with dynamic synapses and shows, in particular, that the self-tuning properties of a circuit with dynamic synapses are a property of the dynamic synapse model and not something hidden in the many details and parameters of a complicated spiking neural network simulation. Every simulation was performed using both the parameters based on experimental data and the R1-R3 dynamic synapse parameters that were derived from our theoretical considerations (see methods). The scaling factors A_{mn} of the dynamic synapses were set only once such that the steady-state dynamic synapse curves intersected at 10Hz. Thus each simulation had identical dynamic synapse parameters. We then perturbed in small increments both the mean and standard deviation of the external input from -50% to $+50\%$ of their normal values ($I^{inject} = 2.455 \times 10^{-9} \text{Amp}$ and noise drawn from a 0-mean Gaussian, $\sigma^{inject} = 6 \times 10^{-9} \text{Amp}$ standard deviation). The results, which are the steady-state excitatory firing rates from the last 1 second of each simulation, are shown in figure 8. All the networks which had a steady-state firing rate between $9-11\text{Hz}$ (a difference of 1Hz or less from the target excitatory firing rate) are denoted by the color blue, networks with firing rates between $8-9\text{Hz}$ and $11-12\text{Hz}$ (a difference between $1-2\text{Hz}$) are shown in cyan and networks with firing rates between $7-8\text{Hz}$ and $12-13\text{Hz}$ (a difference between $2-3\text{Hz}$) are shown in green. In panels A, D, H we show the control case with static synapses for the three different network models for comparison. There were few networks which supported a 10Hz steady-state firing rate. The maximal firing rates were above 40Hz and many networks were essentially shut down with a firing rate very close to or equal to 0Hz. Thus the steady-state firing rates of networks with static synapses are quite dependent on mean current injection and injected noise level. When we ran the same simulations with dynamical synapses turned on (figure 8 remaining panels), the large firing rates were reduced. We examined two different assignments of UDF values to the 4 different types of synaptic connections in the network: Values that are sufficient for inducing stability according to the previously (Results, first section) described analytical approach (panels B, E, H) and values taken from experimental data (panels C, F, I). Interestingly, for this perturbation test the dynamic synapse parameters based on experimental data outperformed somewhat the dynamic synapses parameters based on the analytical approach.

We wish to emphasize that when viewing changes in external input as a perturbation to the network we are examining only the steady-state response of the network and that there is indeed a strong transient response to external input that could provide the excitation necessary for cortical computations, while still allowing for homeostatic regulation on this very short time scale. A transient response to any network perturbation results from the fact that dynamic synapses do not equilibrate instantaneously and thus the response will follow the time scale of the dynamic synapses. This is shown in figure 9 for the case of conductance based spiking networks with dynamic synapse parameters based on the experimental data shown in Table 1 (panels A-C), and R1 dynamic synapse parameters (panels D-F), (the R2 and R3 parameters were similar). Panels A-F show 50ms excitatory firing rate "snapshots" for each network at times 1-50ms, 251-300ms, 451-500ms. Additionally, panel G shows a single network's excitatory and inhibitory response to a constant input with a constant noise variance experimentally observed UDF parameters and panel H shows the same network with R1 dynamic synapse parameters. In the case of experimentally

observed synapse parameters the network compensated for the changed external input in about 600ms resulting in an excitatory steady-state firing rate near 11Hz and an inhibitory steady-state firing rate of 24Hz. In the case of the R1 dynamic synapse parameters the network compensated for the changed external input in about 150ms, resulting in an excitatory steady-state firing rate around 4Hz and an inhibitory steady-state firing rate around 24Hz. This 150ms period is in the same range as the duration of typical transient rate responses to visual stimuli in primary visual cortex (see for example figure 2 in (Lamme and Roelfsema 2000)). The duration of transient rate responses reported for higher visual areas (see e.g. (Rainer et al. 2004)) is somewhat longer, and lies between the durations found in these network simulations for R1 dynamic synapses and dynamic synapses based on experimental data.
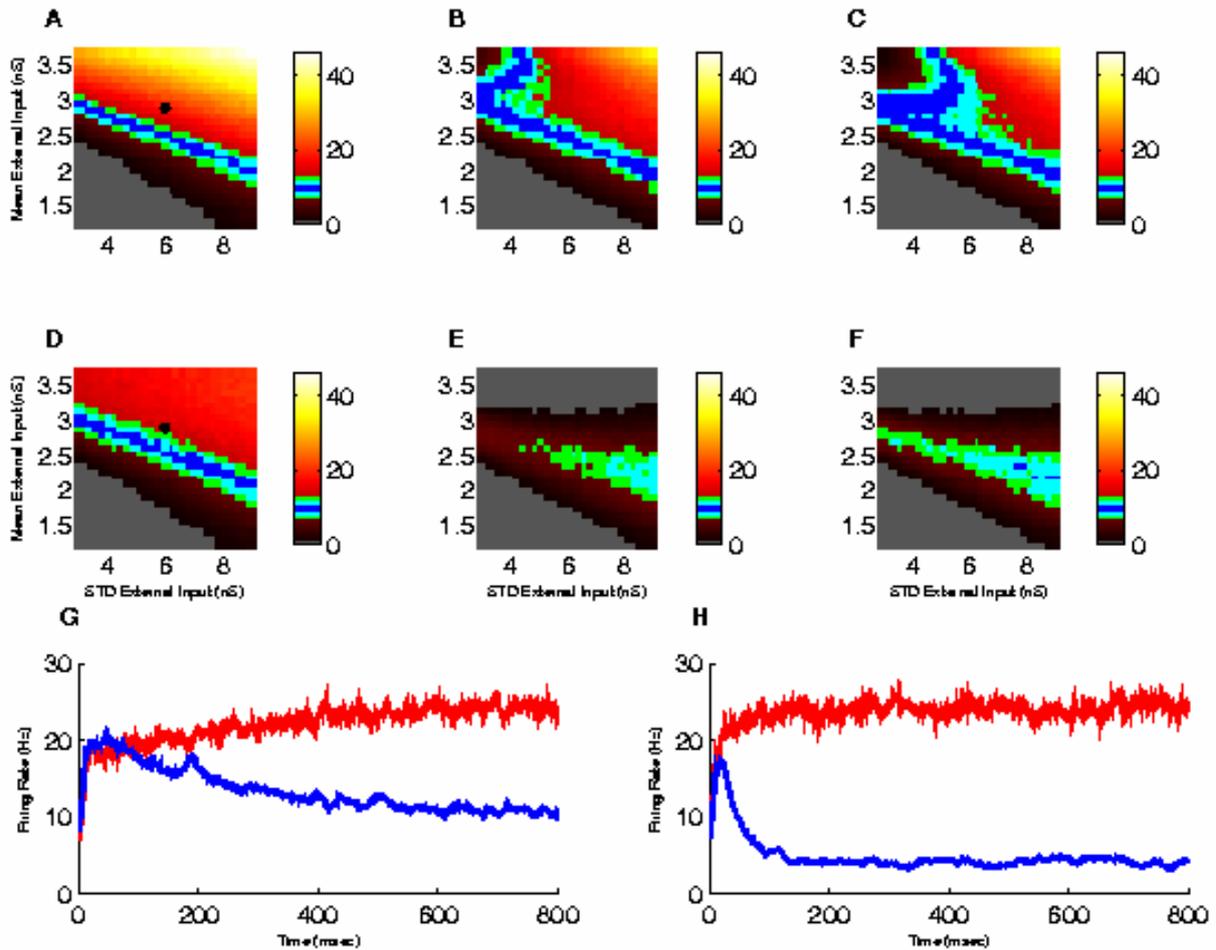

Figure 9 Transient firing rate responses in network models with dynamic synapses. **A-C** Transient firing rate responses for changes in the mean and variance of external inputs are shown for conductance based networks with experimentally observed UDF-parameters for dynamic synapses (see Table 1). A – Firing rate of excitatory neurons during the time interval 1-51ms (in response to a change in external inputs at time 0). The black circle indicates the specific network that is shown in panel G. B – Firing rate of excitatory neurons during 251-300ms, C – 450-500ms. **D-F** The same for conductance based networks using R1 dynamic synapse parameters. **G** – The average firing rate of excitatory (blue) and inhibitory (red) neurons as a function of time (averaged with a 20ms sliding window) for the network represented in panel A as a black dot. **H** – The same for the network represented in panel D as a black dot (the same network with static synapses assumed a steady state firing rate of 19Hz for both excitatory and inhibitory neuron populations, not shown). One sees that in either case the transient firing rate transmitted substantial information about the new level of external input during a significant amount of time after the change in the external input. This suggests that a network-induced homeostasis of firing rates is compatible with computational processes that process information about the change in external inputs.

We examined next the effect of long term changes in synaptic weights on firing rate stability in networks with dynamic synapses. We used the parameter range of static synaptic weight values already shown in figure 5 and assumed that these synaptic weights were a perturbation of some

unknown but correct synaptic weights that would lead to a steady-state firing rate of $10\,\mathrm{Hz}$. Taking each network with it's given, possibly perturbed static synaptic weights, we then used equation (13) to set the synaptic scaling factor for spiking networks with dynamic synapses assuming a target firing rate of $10\,\mathrm{Hz}$. I.e. the A_{mn}, were set to $A_{mn} = J_{mn}/\left(R_{mn}^{*}(10\,\mathrm{Hz})U_{mn}^{1*}(10\,\mathrm{Hz})\right)$, and were thus scaled by a single, constant scale factor across simulations using the same dynamic synapse parameters.

The results of the synaptic weight perturbations for conductance based spiking networks, current based spiking networks and current based mean field models are shown in figure 10.
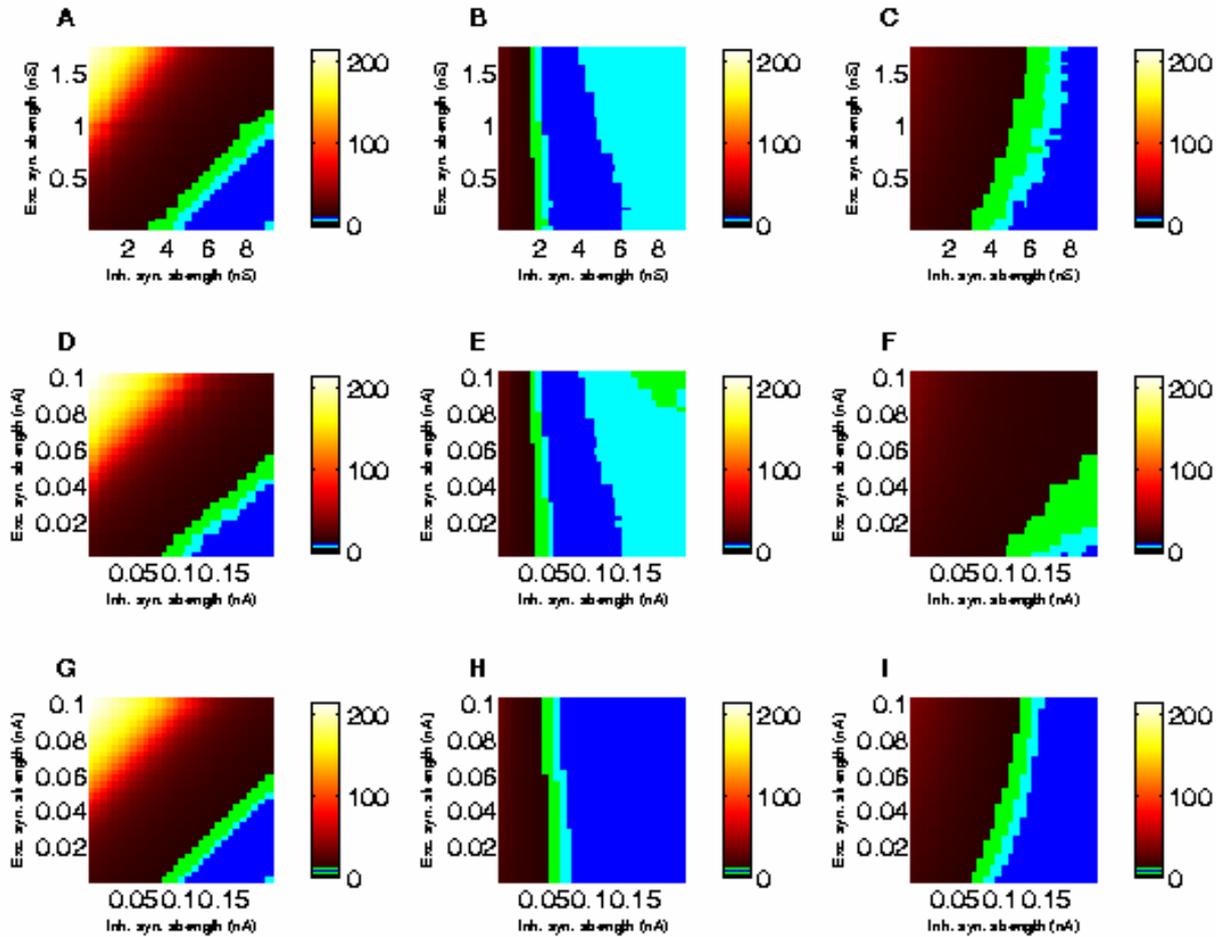

Figure 10 Self-tuning with respect to systematic synaptic strength perturbations. All networks tested were set to a default steady-state firing rate of 10Hz. The color blue denotes the optimal firing rate of 10Hz (between $9\,\mathrm{Hz}$ and $11\,\mathrm{Hz}$), cyan between $8-9\,\mathrm{Hz}$ and $11-12\,\mathrm{Hz}$, green between $7-8\,\mathrm{Hz}$ and $12-13\,\mathrm{Hz}$ and gray denotes networks between $0-1\,\mathrm{Hz}$. The synaptic strength scaling factors A_{mn} for all synaptic perturbations used the same rescaling factor. **A-C** The response (as measured by the steady-state average excitatory firing rate) of the conductance based spiking networks to systematic synaptic strength perturbations. A – The response for spiking conductance based networks with static synapses. B – The response of conductance based spiking networks with dynamic synapses using the R1-R3 parameters. C – The response for conductance based spiking networks with dynamic synapses using the the parameters based on experimental data. **D-F** The response of current based spiking networks to systematic synaptic strength perturbations. D – The response of current based networks with static synapses. E – The response of current based networks with dynamic synapses using the R1-R3 parameters. F – The response of current based networks with dynamic synapses using the parameters based on experimental data. **G-I** The response of current based mean-field firing rate models to systematic perturbations in synaptic strength. G – The response of current based mean-field models with static synapses. H – The response of current based mean-field models with dynamic synapses using the R1-R3 parameters. I – The response of current based mean-field models with dynamic synapses using the the parameters based on experimental data. The mean-field model differs from the current based network in panel F, see footnote 2 for discussion.

In panels A, D, G are the control cases with static synapses, shown for comparison. With static synapses the steady-state firing rates for networks with high excitatory synaptic weights are in excess of 200Hz. However, as shown in panels B, C, E, F, H and I, in networks with dynamic synapses, regardless of conductance based (panels A-C) or current based (D-E) synapses, and regardless of which dynamic synapses parameters are used, the excessive firing rates disappear. Most importantly, in all but the one case of current-based networks with the dynamic synapse parameters based on experimental data, the number of perturbed networks that nevertheless had firing rates very close to the target firing rate increased dramatically. The continuous mean-field predictions of the dynamic synapses applied to the networks with synaptic weight perturbations are shown in panels G-I. The mean-field simulations show excellent performance across nearly the entire range of perturbations and are qualitatively similar to spiking network simulations using dynamic synapses. Network correlation did not play a role in the effect the dynamic synapses had on the networks.

One may notice that some networks which had a firing rate between $9\text{Hz} - 11\text{Hz}$ without dynamic synapses no longer had this firing rate when dynamical synapses were turned on (compare panels D and E, lower left-hand corner). Furthermore, the mean-field model with dynamic synapses (compare panels G and H) expands this range of target firing rates while the current based spiking network does not. Typically, the average excitatory firing rate drops by one or two Hertz when dynamic synapses are turned on in the spiking network. The reason for this is somewhat subtle and it has to do with the spiking networks' synaptic weight values, which are not always in exact agreement with the mean-field model synaptic strength values[4]. While this effect shows up in all three self-tuning results we show, as is clear from the figures, its effect is small, resulting in differences between the spiking networks and the mean-field models of only a few Hertz at most, and the results with dynamic synapses show great improvement over the control case with static synapses, nevertheless.

Why should simply scaling the A_{mn} for dynamic synapses according to equation (13) have a helpful effect on the target firing rate of the network if there is an unknown perturbation of the factor J_{mn} in (13)? Assume for example that there are static synaptic strengths $\left(J_e^*, J_i^*\right)$ that lead to a target firing rate of x^*. Assume further that there is an unknown perturbation of these synaptic strengths that can be written as $\left(J_e^* + \varepsilon_e, J_i^* - \varepsilon_i\right)$. Since we have increased the excitation and decreased the inhibition we should expect an increase in the target firing rate, that is the perturbed synaptic strengths $\left(J_e^* + \varepsilon_e, J_i^* - \varepsilon_i\right)$ lead to $x^* + x_\varepsilon$. If we now examine the same network and synaptic weight perturbation but use dynamic synapses we see a change in behavior. As already outlined we set the A_{mn} according to equation (13), so that $\mu_{me}^*(x^*) = J_e^* + \varepsilon_e$ and $\mu_{mi}^*(x^*) = J_i^* - \varepsilon_i$, because we do not know that there is a perturbation. Now the situation with dynamic synapses is quite different than with static synapses because at x^* the dynamic synapses equilibrate to values that support a higher firing rate than x^*, specifically $x^* + x_\varepsilon$. But at a firing rate of $x^* + x_\varepsilon$, *because the derivatives of the dynamic synapses have the correct signs*, the network supports a firing rate below $x^* + x_\varepsilon$. Thus we can conclude that the firing rate must be between x^* and $x^* + x_\varepsilon$, which is better than the case of static synapses, where the network firing rate is completely dictated by the perturbed synaptic weights and thus has a firing rate of $x^* + x_\varepsilon$. The degree to which the final firing rate will be closer to x^* or $x^* + x_\varepsilon$ depends on the magnitude of these derivatives. We refer to the last part of the Supplementary Material for an analytical comparison of network stability with static and dynamic synapses.
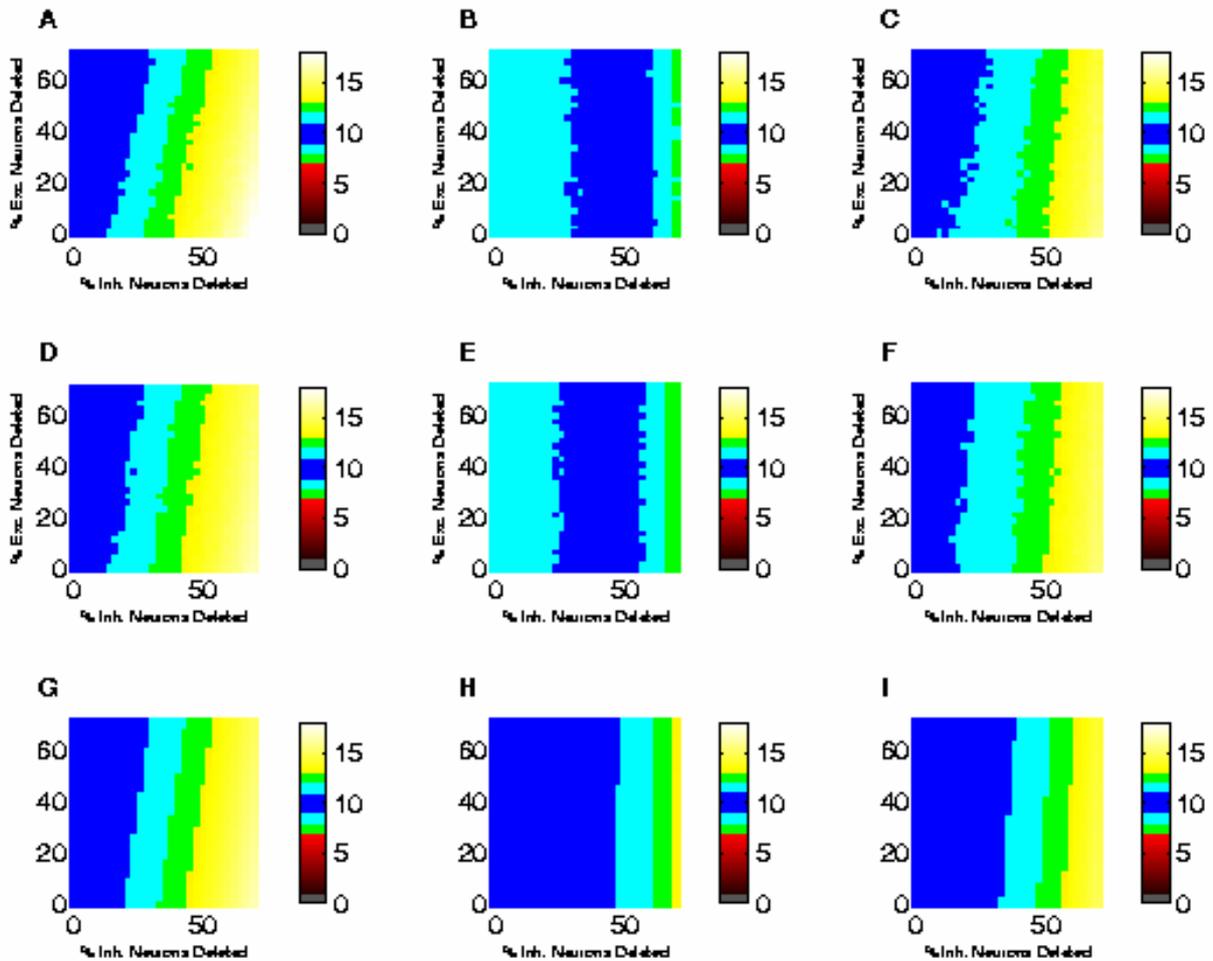
Figure 11 Sparse, spiking networks demonstrate self-tuning with respect to systematic neuron inactivation. All networks tested were set to a default steady-state firing rate of 10Hz. The scaling factors A_{mn} were set only once, thus each set of simulations (a single panel) where dynamic synapses were used, had identical dynamic synapse parameters. The color blue denotes the optimal firing rate of 10Hz (between 9Hz and 11Hz), cyan between $8-9\text{Hz}$ and $11-12\text{Hz}$, green between $7-8\text{Hz}$ and $12-13\text{Hz}$ and gray denotes networks between $0-1\text{Hz}$. **A-C** The response (as measured by the steady-state average excitatory firing rate) of the conductance based spiking networks to systematic neuronal inactivation. A – The response of conductance based spiking networks with static synapses. B – The averaged response of conductance based spiking networks with dynamic synapses using the R1-R3 parameters. C – The response of conductance based spiking networks with the dynamic synapse parameters based on experimental data. **D-F** The response (as measured by the steady-state average excitatory firing rate) of the current based spiking networks to systemic neuronal inactivation. D – The response of current based spiking networks with static synapses. E – The averaged response of current based spiking networks with dynamic synapses using the R1-R3 parameters. F – The response of current based spiking networks with dynamic synapses using the parameters based on experimental data. **G-I** The response (as measured by the steady-state excitatory firing rate) of the current based mean field firing rate models to systemic neuronal inactivation. G – The response of current based mean-field models with static synapses. H – The averaged response of current based mean-field models with dynamic synapses using the R1-R3 dynamic synapse parameters. I – The response of current based mean-field models with dynamic synapses using the parameters based on experimental data.

As a final self-tuning test we also investigated the effects of systematic changes in the excitability of subpopulations of neurons in the simulated circuit. Diverse changes in the excitability of neurons have been reported to be caused by neuromodulators (especially dopamine) in various cortical areas ((Gulledge and Jaffe 1998; 2001), see figure 2B in first reference, for example). Since such changes in the excitability of neurons cannot be modeled directly in the context of LIF neurons, we simply inactivated (i.e., deleted) randomly selected subsets of neurons in the circuit. For continuity, we chose the same networks as in the input perturbation self-tuning

simulation: conductance based spiking networks ($J_{ee} = J_{ie} = 0.4 \times 10^{-9} \text{S}$ and $J_{ei} = J_{ii} = 8.48 \times 10^{-9} \text{S}$), current based spiking networks ($J_{ee} = J_{ie} = 0.013 \times 10^{-9} \text{Amp}$ and $J_{ei} = J_{ii} = -0.18 \times 10^{-9} \text{Amp}$) and the current based mean-field models ($J_{ee} = J_{ie} = 0.013 \times 10^{-9} \text{Amp}$ and $J_{ei} = J_{ii} = -0.18 \times 10^{-9} \text{Amp}$), all with a steady-state firing rate of 10Hz. We randomly chose excitatory and inhibitory neurons in these networks to inactivate, with the total number of inactivated neurons between 0% and 70% of their respective pool totals, in small increments. The current based mean-field model received an analogous perturbation by modifying the K_{mn} parameter in equation (9) according to the neuronal inactivation percentage in the spiking networks. The control simulations with static synapses are shown in figure 11 panels A, D, and G, the results with the R1-R3 dynamic synapse parameters shown in panels B, E, H, and the results with the dynamic synapse parameters based on experimental data in panels C, F and I. For the networks tested, the dynamic synapse parameters based on experimental data did not have a significant effect but the R1-R3 dynamic synapse parameters showed improvement over the control, with the vast majority of networks within 2Hz of the target firing rate of 10Hz. Again, network correlation effects did not play a role in the results of the simulations.
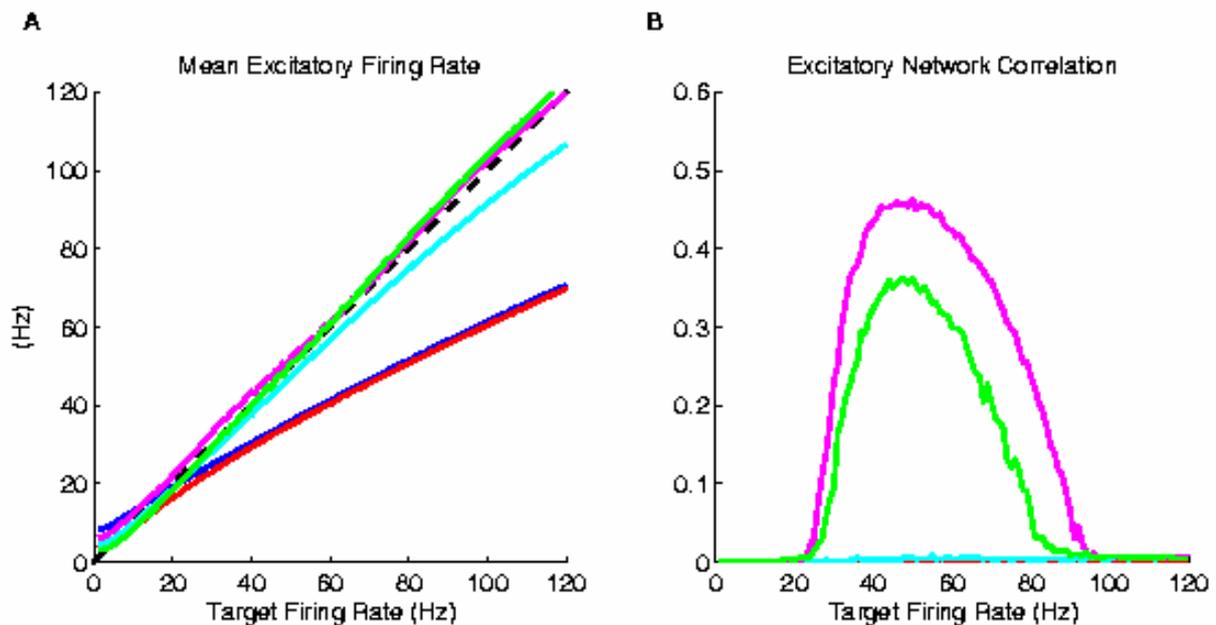

Figure 12 Many spiking networks can follow a target firing rate using dynamic synapses. Five selected current based spiking networks with dynamic synapses showing the networks' abilities to follow an excitatory target firing rate using scaling factors A_{mn} as set by the heuristic of equation (13). The target firing rate was set to every integral firing rate between $1 - 120 \text{Hz}$ and the A s for each network were calculated based on this target frequency. **A** Average target firing rate, the black dashed line shows the line $y = x$, which is optimal performance. The mean absolute error for each network blue, red, cyan, magenta and green are $[20.7, 21.4, 4.5, 2.1, 2.0] \text{Hz}$, respectively. The networks had J_e and J_i as follows (nA): blue $[0.025, -0.05]$, red $[0.025, -0.15]$, cyan $[0.05, -0.1]$, magenta $[0.075, -0.05]$ and green $[0.075, -0.015]$, and are also denoted in figure 5, panel D. The dynamic synapse parameters used were the R1 parameters. **B** Excitatory network correlation as a function of target firing rate. There was negligible network correlation for the blue, red and cyan networks and significant network correlation for the magenta and green networks between the firing rates of 20-100Hz.

Choosing Other Target Firing Rates Implicit in the demonstrated self-tuning properties is the ability to set a specific fixed-point firing rate using dynamic synapses, through the use of the scaling equation (13). The network perturbations then can be viewed as a perturbation away from this fixed point. We thus wondered, in principle, how close a spiking network could get to a

preprogrammed fixed point, as set by equation (13), regardless of what the initial synaptic strengths of the network were. Briefly, we used five networks from the current-based, spiking network synaptic parameter range of figure 5, panel D. The networks had J_e and J_i as follows (nA): blue [0.025,–0.05], red [0.025,–0.15], cyan [0.05,–0.1], magenta [0.075,–0.05] and green [0.075,–0.015] leading to corresponding firing rates of 20Hz, 12Hz, 20Hz, 100Hz, and 20Hz with static synapses. We then chose as the target firing rates every integral firing rate in the range of 1-120Hz and used equation (13) to set the dynamic synapses appropriately in the five networks. We do not mean to suggest that cortical networks create fixed points at such high firing rates, rather only to test the principle behind equation (13). The results, which are the steady-state excitatory firing rates, are shown in figure 12, panel A. All networks showed an ability to enhance their firing rates towards the desired target firing rate, although the two networks with the weakest excitatory synapses (denoted with colors blue and red) were unable to follow the target firing rate closely above 20Hz. Another complication arose in that the two networks with the strongest excitatory synapses (green and magenta), while able to closely follow the target firing rate also showed significant network correlation above 20Hz, shown in panel B. Despite these caveats, the results clearly demonstrate that the ability to tune the steady-state firing rate of a network is a general property of the dynamic synapse configuration. The results lend further evidence to the idea that self-tuning properties of spiking networks with dynamic synapses are caused by setting a firing rate fixed point, to which the networks attempt to return after a perturbation.

Theoretical Analysis There is little hope that one can give a complete theoretical justification for the demonstrated self-tuning properties of sparsely connected circuits of spiking neurons with dynamic synapses, or for the associated mean-field model defined by equations (7) – (9). The reason lies in the nonlinearity of these models, and the fairly large number of variables that are involved. But the demonstrated self-tuning properties of these complex systems are clearly related to known self-tuning properties of substantially simpler systems for which a theoretical analysis is feasible. These analytical results will be discussed in the following.

An Analytical Result on the Assignment of Differential Dynamics to Different Types of Synapses in a Distributed Circuit In the first section of the Results we proposed a heuristic for choosing the signs of the derivatives of the synaptic weight curves $\mu_{mn}^{*}(x_n)$ at x^{*}. We then demonstrated through numerical simulations of circuits of spiking neurons that this choice was justified. This heuristic can also be justified analytically for a two-dimensional mean-field model, similar to that described in equation (11) (assuming dynamic synapses with very small derivatives and instantaneously equilibrating dynamic synapses). One can prove that the derivatives $d_{mn} = \dfrac{d\mu_{mn}}{dx_n}\left(x^{*}\right)$ should have the following signs in order for the excitatory population to have homeostatic properties w.r.t. changes in the intensity of external input currents: $d_{ee} < 0, d_{ii} > 0, d_{ie} > 0, d_{ei} < 0$ (see Supplementary Material for details). These signs agree with the previously proposed heuristic rules for the assignment of depressing and facilitating synapses to the 4 types of synaptic connections (see first section of the Results; note that the negative sign is included in μ_{ei} and μ_{ii}). In order for the excitatory population to have also homeostatic properties w.r.t. changes in the intensity of external input currents to the inhibitory population the analytically derived condition is somewhat more complicated:

$$d_{ee} < 0, d_{ii} > 0, d_{ie} > 0, d_{ei} < 0 \qquad \text{if } \mu_{ee}\left(x^{*}\right) > \frac{1}{\beta_e}$$

$$d_{ee} < 0, d_{ii} < 0, d_{ie} > 0, d_{ei} > 0 \qquad \text{if } \mu_{ee}\left(x^{*}\right) < \frac{1}{\beta_e},$$

where β_e is the derivative of the excitatory FI-curve evaluated at the fixed point x^{*}. Taken together

these conditions imply that regardless of the size of $\mu_{ee}(x^*)$, the $E \to E$ connection should always be depressing and the $E \to I$ should always be facilitating in order to allow the circuit to return to a steady state firing rate in spite of a changed level of external input. Additionally, if $\mu_{ee}(x^*) > \beta_e^{-1}$ the $I \to E$ synapses should be facilitating and the $I \to I$ synapses should be depressing. Otherwise the $I \to E$ synapses should be depressing and the $I \to I$ synapses should be facilitating. The fact that this analytical result does not point to a general rule for the optimal dynamics of synapses from inhibitory neurons (from the perspective of firing rate stability) could be seen as a possible explanation for the diverse distribution of experimentally observed UDF-parameters for these synapses (see panels E and F of figure 4). We additionally give justification for our self-tuning heuristic for the parameter range used in our current based networks in the Supplementary Materials.

A Theoretical Analysis of the Impact of Changes of Synaptic Weights on Stability Properties of Networks with Static and Dynamic Synapses One can prove for the same mean-field model with excitatory and inhibitory neurons that the steady-state firing rate x^* is less affected by small changes in synaptic weights (resulting for example from LTP or LTD) if the synaptic connections are dynamic and tuned using an appropriate heuristic. An analytical derivation is provided in the second part of the Supplementary Material, with specific reference to the fact that our self-tuning heuristic is appropriate for the parameter regime used in the current based spiking networks in this paper. An additional example figure (S1) is also given.

Discussion

We have shown that the inclusion of more realistic models for synapses, which reflect their experimentally found short-term plasticity, provides models for cortical neural networks with interesting stability properties. In particular, it enables such models to return after a large variety of perturbations to a low but non-zero spontaneous firing rate, even if the perturbation, such as a change in the level of external input, a change in synaptic strength, or even neuron deletion, is of a longer lasting nature. This surprising stability property of network models with dynamic synapses, which can apparently not been reproduced in models with static synapses, may provide a possible explanation for the surprisingly stable low but non-zero rate of spontaneous firing that has been reported for cortical neurons in a variety of studies. Several other homeostatic processes, such as synaptic scaling, LTP and LTD and genetic regulation of receptor numbers are likely to support the stability of the rate of spontaneous firing of cortical neurons on a larger time scale (Turrigiano and Nelson 2004). But none of these mechanisms would apparently be able to support stability on the time scale of seconds, for example in response to a changed level of sensory input, or to a changed concentration of neuromodulators in a cortical circuit. On the other hand we have shown in figure 9 that the stability property endowed by short-term synaptic plasticity leaves a sufficiently large time window of one to several hundred milliseconds during which the firing rate in the circuit is affected by the external perturbation. Hence information about such external inputs can be transmitted to other cortical circuits, and integrated into cortical computation. In fact, the dynamic response to an increased external input shown in panel H of figure 9 is on a similar time scale as typical responses to visual inputs in primary visual cortex (see for example figure 2 in (Lamme and Roelfsema 2000). But even on a larger time scale, the information about the external (or internal) perturbation remains accessible to the neural system, although the firing rate of excitatory neurons is returned through synaptic dynamics to a given target level. The same firing rate of excitatory neurons is then accompanied by a different firing rate of inhibitory neurons (see panels G and H in figure 9), and this rate may therefore contain substantial information about the nature and level of the external perturbation for a much longer time period. This observation also implies that the same firing rate of excitatory neurons can be produced by a virtually infinite combination of concentration levels of neuromodulators and activity levels of inhibitory neurons, analogously to the large sets of different

circuit parameters that have been reported to support the generation of a target firing pattern in the pyloric circuit in the crustacean stomatogastric ganglion (Marder and Goaillard 2006).

The target value of 10 Hz for the spontaneous firing rate excitatory neurons in cortical circuits on which we have focused in our network simulations was chosen rather arbitrary, although it lies within a range of spontaneous firing rates that has been reported in number of experimental studies (see Introduction). We have shown in figure 12 that a large range of other target values can be achieved by choosing a suitable global scaling parameter for synaptic weights, which might for example be under genetic control. However in order to demonstrate stability at really low rates (say 1 Hz), one needs to add neuron models to the network that fire spontaneously even in the absence of synaptic input (or during a release from inhibition). Otherwise the network cannot recover from a temporary pause in firing, and will remain indefinitely silent.

We have shown in this article that the stability of the firing rate of excitatory neurons endowed by short-term synaptic dynamics is rooted in general principles of control theory, which have recently been proposed for much simpler dynamical systems. In fact, activity dependent rescaling of feedback strength has been postulated as a powerful mechanism for self-tuning in control theory for purely mathematical reasons (Moreau and Sontag, 2003). We have demonstrated that this theoretical analysis of stability properties provided by dynamic synapses can be extended to the case of a distributed system that consists of several interacting dynamical modules, such as an interacting population of excitatory and inhibitory neurons in a cortical circuit, each with thousands of neurons. In particular, we have exhibited an analytical method for deriving rules regarding the type of synaptic dynamics that should be assigned to different types of synapses for the purpose of network stability. This theoretical approach may help to provide an explanation for the diversity of the empirically found short-term plasticity of connections between modules with different dynamic roles (such as excitatory and inhibitory neurons). It turns out that this theoretical analysis provides clearer predictions for the dynamics of synapses from excitatory neurons than for GABAergic synapses. This might provide an explanation for the experimentally found diversity in the dynamics of GABAergic synapses.

Finally we would like to emphasize that the investigation of the relationship between stability properties of networks of spiking neurons and the dynamics of specific types of synapses that we have initiated in this article should only be seen as a first step. In a second step one needs to investigate through computer simulations also more detailed network models consisting of different types of excitatory and especially inhibitory neurons with specific firing properties and more specific connectivity patterns. A quite challenging open problem is whether one can also extend the theoretical analysis of stability properties induced by dynamic synapses to more complex networks.

Acknowledgements

Grants

References

Abbott LF, and Nelson SB. Temporal dynamics of biological synapses. In: *The Handbook of Brain Theory and Neural Networks*, edited by Arbib MAMIT Press, 2003, p. 1156-1158.

Abbott LF, and Regehr WG. Synaptic computation. *Nature* 431: 796-803, 2004.

Abbott LF, Varela JA, Sen K, and Nelson SB. Synaptic depression and cortical gain control. *Science* 275: 220-224, 1997.

Abeles M. *Corticonics: Neural Circuits of the Cerebral Cortex*. Cambridge University Press, 1991.

Baddeley R, Abbott LF, Booth MC, Sengpiel F, Freeman T, Wakeman EA, and Rolls ET. Responses of neurons in primary and inferior temporal visual cortices to natural scenes. *Proceedings* 264: 1775-1783, 1997.

Brunel N. Dynamics of sparsely connected networks of excitatory and inhibitory spiking neurons. *Journal of computational neuroscience* 8: 183-208, 2000.

Buzsaki. *Rhythms of the Brain*. Oxford University Press, 2006.

Destexhe A, and Contreras D. Neuronal computations with stochastic network states. *Science* 314: 85-90, 2006.

Destexhe A, Rudolph M, and Pare D. The high-conductance state of neocortical neurons in vivo. *Nature reviews* 4: 739-751, 2003.

Galarreta M, and Hestrin S. Frequency-dependent synaptic depression and the balance of excitation and inhibition in the neocortex. *Nature neuroscience* 1: 587-594, 1998.

Gulledge AT, and Jaffe DB. Dopamine decreases the excitability of layer V pyramidal cells in the rat prefrontal cortex. *J Neurosci* 18: 9139-9151, 1998.

Gulledge AT, and Jaffe DB. Multiple effects of dopamine on layer V pyramidal cell excitability in rat prefrontal cortex. *Journal of neurophysiology* 86: 586-595, 2001.

Gupta A, Wang Y, and Markram H. Organizing principles for a diversity of GABAergic interneurons and synapses in the neocortex. *Science* 287: 273-278, 2000.

Haeusler S, and Maass W. A Statistical Analysis of Information-Processing Properties of Lamina-Specific Cortical Microcircuit Models. *Cereb Cortex* 2006.

Lamme VA, and Roelfsema PR. The distinct modes of vision offered by feedforward and recurrent processing. *Trends in neurosciences* 23: 571-579, 2000.

Legenstein R, and Maass W. Edge of chaos and prediction of computational performance for neural microcircuit models. *Neural Networks* in press: 2007.

Lisman JE. Bursts as a unit of neural information: making unreliable synapses reliable. *Trends in neurosciences* 20: 38-43, 1997.

Maass W, Natschlager T, and Markram H. Fading memory and kernel properties of generic cortical microcircuit models. *Journal of physiology, Paris* 98: 315-330, 2004.

Marder E, and Goaillard JM. Variability, compensation and homeostasis in neuron and network function. *Nature reviews* 7: 563-574, 2006.

Markram H, Wang Y, and Tsodyks M. Differential signaling via the same axon of neocortical pyramidal neurons. *Proceedings of the National Academy of Sciences of the United States of America* 95: 5323-5328, 1998.

Moreau L, and Sontag E. Balancing at the border of instability. *Physical review* 68: 020901, 2003a.

Moreau L, and Sontag E. Feedback tuning of bifurcations. *System Control Letters* 50: 229-239, 2003b.

Rainer G, Lee H, and Logothetis NK. The effect of learning on the function of monkey extrastriate visual cortex. *PLoS biology* 2: E44, 2004.

Shriki O, Hansel D, and Sompolinsky H. Rate models for conductance-based cortical neuronal networks. *Neural computation* 15: 1809-1841, 2003.

Steriade M. *The Intact and Sliced Brain*. MIT Press, 2001.

Steriade M, Timofeev I, and Grenier F. Natural waking and sleep states: a view from inside neocortical neurons. *Journal of neurophysiology* 85: 1969-1985, 2001.

Thomson AM. Activity-dependent properties of synaptic transmission at two classes of connections made by rat neocortical pyramidal axons in vitro. *The Journal of physiology* 502 (Pt 1): 131-147, 1997.

Thomson AM. Presynaptic frequency- and pattern-dependent filtering. *Journal of computational neuroscience* 15: 159-202, 2003.

Tsodyks M, Pawelzik K, and Markram H. Neural networks with dynamic synapses. *Neural computation* 10: 821-835, 1998.

Turrigiano GG, and Nelson SB. Homeostatic plasticity in the developing nervous system. *Nature reviews* 5: 97-107, 2004.

van Vreeswijk C, and Sompolinsky H. Chaos in neuronal networks with balanced excitatory and inhibitory activity. *Science* 274: 1724-1726, 1996.

van Vreeswijk C, and Sompolinsky H. Chaotic balanced state in a model of cortical circuits. *Neural computation* 10: 1321-1371, 1998.

Varela JA, Sen K, Gibson J, Fost J, Abbott LF, and Nelson SB. A quantitative description of short-term plasticity at excitatory synapses in layer 2/3 of rat primary visual cortex. *J Neurosci* 17: 7926-7940, 1997.

Vogels TP, and Abbott LF. Signal propagation and logic gating in networks of integrate-and-fire neurons. *J Neurosci* 25: 10786-10795, 2005.

Vogels TP, Rajan K, and Abbott LF. Neural network dynamics. *Annual review of neuroscience* 28: 357-376, 2005.

Wang Y, Markram H, Goodman PH, Berger TK, Ma J, and Goldman-Rakic PS. Heterogeneity in the pyramidal network of the medial prefrontal cortex. *Nature neuroscience* 9: 534-542, 2006.

Yoshimura Y, and Callaway EM. Fine-scale specificity of cortical networks depends on inhibitory cell type and connectivity. *Nature neuroscience* 8: 1552-1559, 2005.

Yoshimura Y, Dantzker JL, and Callaway EM. Excitatory cortical neurons form fine-scale functional networks. *Nature* 433: 868-873, 2005.

Footnotes

[1] It is shown in (Moreau and Sontag, 2003) that it suffices to assume that

- f is decreasing
- g is strictly increasing
- there exists some $x*$ such that $f\left(x*\right) = g\left(\mu_0\right)$.

[2] The variable u_{k-1} in the third equation of (3) had been erroneously replaced by u_k in **Markram H, Wang Y, and Tsodyks M**. Differential signaling via the same axon of neocortical pyramidal neurons. *Proceedings of the National Academy of Sciences of the United States of America* 95: 5323-5328, 1998., see the discussion in **Maass W, and Markram H.** Synapses as dynamic memory buffers. *Neural Networks* 15:155-161, 2002.

[3] Please see the Supplemental Materials for a theoretical justification of these choices.

[4] In a spiking network without dynamic synapses there is a distribution of firing rates, whose mean we have used as the steady-state firing rate of the network. In these networks even the tails of the neuronal firing rate distribution have the same synaptic weight values J_{mn}. However, in the spiking network with dynamic synapses turned on, the lower part of the firing rate distribution will typically have synapses that are stronger than the set value $\mu_{mn}(x^*) = J_{mn}$ for the target firing rate and the higher part of the distribution will typically have synapses that are weaker then J_{mn}. Since the steady-state dynamic synapse efficacy curves were constructed only to make sure the derivatives had the right signs there is no reason that the expected value of the steady-state synaptic weight across all synapses from neuron type n to m should exactly equal the mean-field average, i.e. that $\int P(x_n)\mu_{mn}^*(x_n) = J_{mn}$, where $P(x_n)$ is the distribution of firing rates for neuron type n. Furthermore, changing the target firing rate may change the shape of the steady-state firing rate distribution of the network, thus making it effectively impossible to cancel this effect if one desires to tune the same network to different firing rates. Overall, this effect results in no more than a 1-2Hz difference between the mean-field prediction of the effect of dynamic synapses and the spiking network results with dynamic synapses.

Supplementary Material

An Analytical Result on the Assignment of Differential Dynamics to Different Types of Synapses in a Distributed Circuit: Conditions on Derivatives of $\mu_{mn}^{*}(x_n)$ at x^{*}. In this supplementary material, we simplify the model in order to analytically calculate whether facilitating or depressing connections are better to achieve homeostatic control at a steady state firing rate. In particular, we study the two-population mean-field model described by

$$\tau_m \frac{dx_m}{dt} = -x_m + f_m\left(v_m + \sum_{n=e,i} \mu_{mn}^{*}(x_n)x_n \right), \tag{S1}$$

where $\vec{x} = \begin{pmatrix} x_e \\ x_i \end{pmatrix}$ are the firing rates of excitatory and inhibitory population, $\vec{v} = \begin{pmatrix} v_e \\ v_i \end{pmatrix}$ is the external input to excitatory and inhibitory population, the index $m = e,i$ means either excitatory or inhibitory population, and f_m is a monotonically increasing f-I curve of excitatory or inhibitory population. The dynamical synapses, $\mu_{mn}^{*}(x_n)$, are modeled to be a function of their pre-synaptic firing rate only, i.e. they are instantly equilibrating.

Let $\vec{x}^{*}$ be a fixed point of the equation (S1), which satisfies the fixed point condition

$$x_m^{*} = f_m\left(v_m + \sum_{n=e,i} \mu_{mn}^{*}(x_n^{*})x_n^{*} \right). \tag{S2}$$

Now, we apply perturbation theory and calculate how much an additional small current injection, $\delta\vec{v}$, to the system shifts the fixed point and how the dynamical synapses contribute to this shift. The shift in the output firing rates, $\delta\vec{x}$, is described by

$$x_m^{*} + \delta x_m = f_m\left(v_m + \delta v_m + \sum_{n=e,i} \mu_{mn}^{*}(x_n^{*} + \delta x_n)[x_n^{*} + \delta x_n] \right). \tag{S3}$$

Linearization of equation (S3) around the old fixed point $\vec{x}^{*}$ gives, up to the first order of $\delta\vec{x}$,

$$\delta x_m = \beta_m\left[\delta v_m + \sum_{n=e,i}\left(J_{mn}\delta x_n + d_{mn}\delta x_n x_n^{*} \right) \right], \tag{S4}$$

where $J_{mn} = \mu_{mn}^{*}(x_n^{*})$, $d_{mn} = d\mu_{mn}(x_n^{*})/dx_n^{*}$ and we introduce the slope of f-I curve,

$$\beta_m = f_m{}'\left(v_m + \sum_{n=e,i} J_{mn}x_n^{*} \right),$$

evaluated at the old fixed point $\vec{x}^{*}$. Using some matrix notation $\beta = \begin{pmatrix} \beta_e & 0 \\ 0 & \beta_i \end{pmatrix}$, $\tilde{J}_{mn} = \beta_m J_{mn}$, and $\tilde{D}_{mn} = \beta_m d_{mn} x_n^{*}$, we can solve for $\delta\vec{x}$ in equation (S4) in the following way:

$$\delta\vec{x} = \beta\delta\vec{v} + \left(\tilde{J} + \tilde{D}\right)\delta\vec{x}$$
$$= \left[I - (\tilde{J} + \tilde{D})\right]^{-1}\beta\delta\vec{v}. \tag{S5}$$

Therefore, the perturbations in the fixed point firing rates $\delta \vec{x}$, caused by the additional current injection $\delta \vec{v}$, are derived from equation (S5).

In the following, we study whether facilitating or depressing synapses are better to achieve smaller changes in the fixed point firing rate of the excitatory population, δx_e, compared with the static synapse case ($\tilde{D}_{mn} = 0$). To do so, we assume that the dynamic synapses are nearly static ($\tilde{D}_{mn} \approx 0$) and evaluate $\dfrac{\delta x_e}{\delta v_e}$ and $\dfrac{\delta x_e}{\delta v_i}$ up to the first order of $\tilde{D}_{mn}$. After some calculations, we obtain

$$\frac{\delta x_e}{\delta v_e} = \frac{\beta_e (1+|\tilde{J}_{ii}|)}{\alpha}\left[1 + \frac{(1+|\tilde{J}_{ii}|)\tilde{D}_{ee}}{\alpha} - \frac{|\tilde{J}_{ei}|\tilde{J}_{ie}\tilde{D}_{ii}}{\alpha(1+|\tilde{J}_{ii}|)} - \frac{|\tilde{J}_{ei}|\tilde{D}_{ie}}{\alpha} + \frac{\tilde{J}_{ie}\tilde{D}_{ei}}{\alpha}\right] + O(\tilde{D}^2)$$

$$\frac{\delta x_e}{\delta v_i} = \frac{-\beta_i|\tilde{J}_{ei}|}{\alpha}\left[1 + \frac{(1+|\tilde{J}_{ii}|)\tilde{D}_{ee}}{\alpha} + \frac{(1-\tilde{J}_{ee})\tilde{D}_{ii}}{\alpha} - \frac{|\tilde{J}_{ei}|\tilde{D}_{ie}}{\alpha} - \frac{(1-\tilde{J}_{ee})(1+|\tilde{J}_{ii}|)\tilde{D}_{ei}}{\alpha|\tilde{J}_{ei}|}\right] + O(\tilde{D}^2),$$

(S5)

where $\alpha = (1-\tilde{J}_{ee})(1+|\tilde{J}_{ii}|) + |\tilde{J}_{ei}||\tilde{J}_{ie}|$. Note that, from the monotonically increasing property of the f-I curves, $\beta_m > 0$; If we assume the stability of the old fixed point $\vec{x}^*$ in the absence of the dynamical synapses, $\alpha > 0$. Hence, looking at equation (S5) term by term, in order to decrease the shift caused by δv_e, we obtain

$$\tilde{D}_{ee} < 0, \tilde{D}_{ii} > 0, \tilde{D}_{ie} > 0, \tilde{D}_{ei} < 0. \tag{S6}$$

To decrease the shift caused by δv_i, we have the same condition,

$$\tilde{D}_{ee} < 0, \ \tilde{D}_{ii} > 0, \ \tilde{D}_{ie} > 0, \ \tilde{D}_{ei} < 0 \qquad \text{if} \qquad \tilde{J}_{ee} > 1, \tag{S7}$$

but different condition

$$\tilde{D}_{ee} < 0, \ \tilde{D}_{ii} < 0, \ \tilde{D}_{ie} > 0, \ \tilde{D}_{ei} > 0 \qquad \text{if} \qquad \tilde{J}_{ee} < 1. \tag{S8}$$

These conditions imply that the $E \to E$ connections should always be depressing and $E \to I$ connections should always be facilitating to have better homeostatic properties. On the other hand, the $I \to I$ connections should be depressing and the $I \to E$ connections should be facilitating if $\mu_{ee}^*\left(x_e^*\right) > 1/\beta_e$ (rephrased from $\tilde{J}_{ee} > 1$) but they should have the opposite properties if $\mu_{ee}^*\left(x_e^*\right) < 1/\beta_e$.

In the simulations shown in the main text we injected the same current to both the inhibitory and excitatory populations (i.e. $v_e = v_i = v$.) Additionally, we had $J_{ee} = J_{ei} = J_e$, $J_{ei} = J_{ii} = J_i$. We used the same FMS-surface, which is equivalent to using the same FI-curve, thus $f_e = f_i = f$, which implies $\beta_e = \beta_i = \beta$. In order to see whether conditions (S7) or (S8) are correct for the networks in the main text we add term-by-term both equations in (S5) and examine the signs of each term in front of $\tilde{D}_{mn}$. After some calculation this gives to first order:

$$\frac{\delta x_e}{\delta v_e} + \frac{\delta x_e}{\delta v_i} = \left(\frac{\beta}{\alpha}\right) + \frac{\beta}{\alpha^2}\left((1+|\tilde{J}_i|)\tilde{D}_{ee} - |\tilde{J}_i|\tilde{D}_{ii} - |\tilde{J}_i|\tilde{D}_{ie} + (1+|J_i|)\tilde{D}_{ei}\right) \tag{S8B}$$

which, based on the signs of the $\tilde{D}_{mn}$ coefficients, shows that the $E \to E$ and $I \to I$ connections should be depressing and the $E \to I$ and $I \to E$ connections should be

facilitating in order to have optimal homeostatic properties with respect to the parameters used in the main text.

A Theoretical Analysis of the Impact of Changes of Synaptic Weights on the Stability Properties of Networks with Static and Dynamic Synapses: Comparison of $\delta x_m / \delta J_{kl}$ **for Static and Dynamic synapses** We present an additional argument, which explains the stability of firing rates (in circuits of spiking neurons with dynamic synapses) with regard to changes in the scaling of synaptic weights. This stability was demonstrated in figure 10 panels B, C, E, F, H, and I, and it was shown in figure 10 panels A, D, G that the control circuits with static synapses do not share this stability property.

It can be easily seen that the previous analysis, which determined the conditions on the derivatives in order to achieve homeostatic properties of the excitatory firing rate with respect to a perturbation in the input current v_m, can be applied in a similar fashion to show that the same conditions achieve homeostatic properties of the excitatory population with respect to a perturbation δJ_{mn} in the synaptic weights $J_{mn} = \mu_{mn}^{*}(x_n^{*})$. Said differently, the conditions given in the previous section provide networks with dynamic synapses better homeostatic properties over the similar networks, with respect to synaptic weight perturbations. To see this we simply rewrite equation (S3) for a perturbation in synaptic strengths, which gives

$$x_m^{*} + \delta x_m = f_m\left(v_m + \sum_{n=e,i}\left(J_{mn} + \delta J_{mn} + d_{mn}\delta x_n\right)[x_n^{*} + \delta x_n]\right) \qquad (S9)$$

Linearization of equation (S9) around the old fixed point $\vec{x}^{*}$ gives, up to the first order of $\delta\vec{x}$,

$$\delta x_m = \beta_m\left[\sum_{n=e,i}\delta J_{mn}x_n^{*} + \sum_{n=e,i}\left(J_{mn}\delta x_n + d_{mn}\delta x_n x_n^{*}\right)\right], \qquad (S10)$$

To see the similarity between equation (S10) and equation (S4) we set $\delta v_m = \sum_{n=e,i}\delta J_{mn}x_n^{*}$ and observe that $\delta x_m / \delta J_{kl} = \delta x_m / \delta v_k x_l^{*}$ (here we use indices k and l to denote all J, irrespective of neuronal population). This quantity $\delta x_m / \delta J_{kl}$ tells us how a small change in J_{kl}, δJ_{kl}, leads to a corresponding small change in the fixed points of the system, $\delta x_m = x_m - x_m^{*}$. We conclude that conditions for homeostatic properties for the perturbations $\delta x_m / \delta J_{kl}$ are derived from the homeostatic properties for the perturbations $\delta x_m / \delta v_m$, assuming again that the d_{mn} are small.

We show now that the heuristic proposed in the first section of the Results in the main text is appropriate to reduce a perturbation of x_e w.r.t. synaptic perturbations for the current based networks. The relevant assumptions are $v_e = v_i = v$, $J_{ee} = J_{ei} = J_e$, $J_{ei} = J_{ii} = J_i$ and $f_e = f_i = f$, which implies $\beta_e = \beta_i = \beta$. Observe that

$$\frac{\delta x_e}{\delta J_e} = \frac{\delta x_e}{\delta J_{ee}} + \frac{\delta x_e}{\delta J_{ei}} = \left(\frac{\delta x_e}{\delta v_e} + \frac{\delta x_i}{\delta v_i}\right)x_e^*, \text{ and similarly } \frac{\delta x_e}{\delta J_i} = \left(\frac{\delta x_e}{\delta v_e} + \frac{\delta x_i}{\delta v_i}\right)x_i^*.$$ These last expressions are proportional to the two quantities in expression (S5) and so our previous analysis leading to (S8B) shows that heuristics used in the main paper are optimal for self-tuning of the excitatory population to perturbations in the synapse strengths J_e and J_i.

Finally, we provide in the following an example and show that $\delta x_m / \delta J_{kl}$ (now for a general δJ_{kl}) for model S1 with dynamic synapses is less than $\delta x_m / \delta J_{kl}$ for model (S1) with static synapses $d_{mn} = 0$. For further simplicity assume that in equation (S1) the FI-curves are identical and linear with slope β and that the $\mu_{mn}^*(x_n)$ are simply linear functions of the pre-synaptic firing rate written as $\mu_{mn}^*(x_n) = d_{mn}(x_n - x_n^*) + J_{mn}$ so that both systems have synaptic weights J_{kl} at the fixed point (x_e^*, x_i^*). Under this assumption, we wish to calculate the quantity $\delta x_m / \delta J_{kl}$ for systems with static and dynamic synapses and then compare their absolute values. First we compute the fixed points of both models. These are

$$x_e^* = \beta v \frac{\left(1 + \beta|J_{ii}| - \beta|J_{ei}|\right)}{\left(1 - \beta J_{ee}\right)\left(1 + \beta|J_{ii}|\right) + \beta^2|J_{ei}|J_{ie}},$$

$$x_i^* = \beta v \frac{\left(1 - \beta J_{ee} + \beta J_{ie}\right)}{\left(1 - \beta J_{ee}\right)\left(1 + \beta|J_{ii}|\right) + \beta^2|J_{ei}|J_{ie}}.$$

A first order perturbation around the fixed point allows us to calculate the desired quantities $\delta x_m / \delta J_{kl}$ for each model. We compute $\delta x_m / \delta J_{kl}$, using a first order expansion around $\vec{x}^*$ and J:

$$\delta\vec{x} = \left[I - \left(\tilde{J} + \tilde{D}\right)\right]^{-1}\beta\delta J\vec{x}^*$$

$$\frac{\delta x_m}{\delta J_{kl}} = \left[I - \left(\tilde{J} + D\right)\right]^{-1}_{mk}\beta\delta x_l^*,$$

so we have everything we need now to calculate and compare the $\delta x_m / \delta J_{kl}$ values between the dynamic synapse model and the static synapse model ($\tilde{D}$ has zeros only) for systematically varied values of J_{kl}, which is shown in figure S1. This example shows for the same perturbation in static synapse weights J_{kl}, the fixed point of model S1 with firing-rate dependent synaptic weights with conditions given by equations (S6) is perturbed less than the fixed point of the same model with static weights.
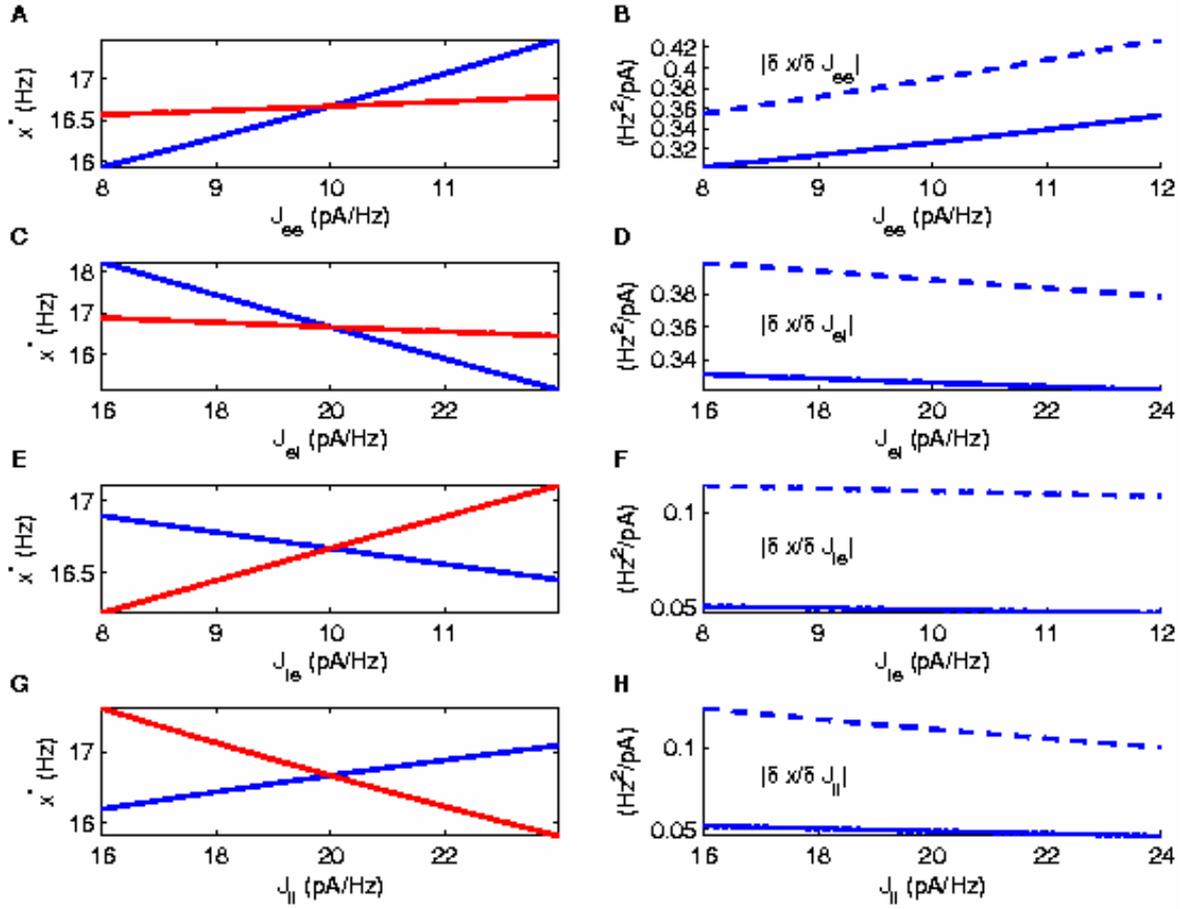
Figure S1 Firing-rate dependent synaptic weights confer robustness to perturbations in static synaptic strength. A system with pre-synaptic firing rate dependent synaptic weights is has an excitatory population that is more robust to perturbations of synaptic weights than the same system with static synapses. **A** Firing rates of system while varying the static synapse weight parameter J_{ee} (blue x_e^*, red x_i^*). **B** Perturbations of the static synapse strength J_{ee} lead to smaller changes in the firing rate for the system with firing rate dependent synaptic strengths. The computation of $\delta x_e / \delta J_{kl}$, for a system with static and dynamic synapses as a function of J_{ee} . The absolute value $\left| \delta x_e / \delta J_{kl} \right|$ is shown. The blue solid line shows the system with dynamic synapses and the dashed line shows the system with static synapses. **C, D** Same as A,B but for J_{ei} . **E, F** Same as A,B but for J_{ie} . **G, H** Same as A,B but for J_{ii} . All systems are locally stable in the ranges shown.

$$\left(J_{ee} = 10\,\text{pA/Hz}, \left| J_{ei} \right| = 20\,\text{pA/Hz}, J_{ie} = 10\,\text{pA/Hz}, \left| J_{ii} \right| = 20\,\text{pA/Hz} \right).$$ Each synaptic weight was individually varied between 0.8 and 1.2 times its base value while other synaptic weights were held constant.

The derivatives were set to $\left(d_{ee} = -0.5\,\text{pA/Hz}^2, d_{ei} = -0.5\,\text{pA/Hz}^2, d_{ie} = 0.5\,\text{pA/Hz}^2, d_{ii} = 0.5\,\text{pA/Hz}^2 \right)$ and $\beta = 20\,\text{Hz/nA}$, with input $v_e = v_i = 1\,\text{nA}$.